Numerical investigation of Landau damping in dynamical Lorentz gases

Thierry Goudon, Léo Vivion

Numerical investigation of Landau damping in dynamical Lorentz gases

Thierry Goudon[a,*], Léo Vivion[a]

[a]Université Côte d'Azur, Inria, CNRS, LJAD, Parc Valrose, F-06108 Nice, France

ARTICLE INFO

Keywords:
Vlasov–like equations
Interacting particles
Landau damping
Inelastic Lorentz gas
Finite elements and semi-Lagrangian schemes

ABSTRACT

We investigate numerically the behavior of a particle, or a set of particles, which exchange momentum and energy with the environment, described as a transverse vibrational field. The large time behavior is characterized, in some specific circumstances, by means of effective friction force and Landau damping. In order to discuss these issues on numerical grounds, we set up a dedicated numerical method. The scheme couples a Finite Element Method for the wave equation, with an appropriate transparent boundary condition that preserves the dispersive effects driving the asymptotic behavior of the system, and a symplectic scheme or a Semi-Lagrangian method for the evolution of the particles. The time discretisation is constructed to capture accurately the energy exchanges. The numerical simulations shed new light on the theoretical results and bring out clearly the role of the parameters of the models.

1. Introduction

This paper is devoted to the numerical investigation of equations modeling the interaction of particles with their environment, according to a description originally introduced by L. Bruneau & S. de Bièvre [5]. We refer the reader to Fig. 1 for a rough picture that can guide the intuition on this description. Particles evolve in the physical space $\mathbb{R}^d$, and the behavior of the environment is embodied into a vibration field which waves in the transverse direction $\mathbb{R}^n$. The motion space and the vibration space are distincts and there is no a priori relation between n and d. The environment can be thought of as a (continuum) set of membranes, activated by the passage of the particles, as depicted in Fig. 1, and on each position $x \in \mathbb{R}^d$, the particles can exchange momentum and energy with the membranes.

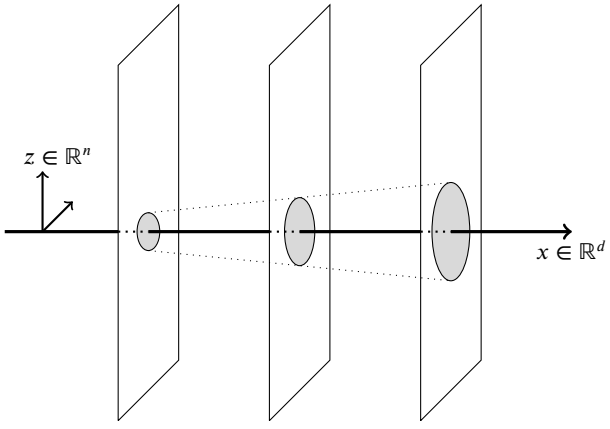

Figure 1: Particle-wave interactions

The interaction is thus driven by the following parameters:

- two form functions $x \in \mathbb{R}^d \mapsto \sigma_1(x)$ and $z \in \mathbb{R}^n \mapsto \sigma_2(z)$ determine the interaction domain, in the physical and the transverse directions respectively, between the particles and the waves; they are both non negative, spherically symmetric, infinitely smooth and compactly supported;
- the vibration field is characterized by the (uniform) wave speed $c > 0$.

As we shall see below, the dimension n of the vibrational direction plays also a fundamental role.

The behavior of a *single particle* governed by this dynamics is discussed in [5]: with $q(t)$ denoting the position of the particle, and $\psi(t, x, z)$ describing the environment, one considers the system

$$\ddot{q}(t) = -\nabla W(q(t)) - \iint_{\mathbb{R}^d\times\mathbb{R}^n} \sigma_1(q(t) - y)\sigma_2(z)\nabla_y\psi(t, y, z)\,\mathrm{d}y\,\mathrm{d}z, \tag{1a}$$

$$\partial_{tt}^2\psi - c^2\Delta_z\psi = -\sigma_2(z)\sigma_1(x - q(t)), \tag{1b}$$

for $t \geq 0$, $x \in \mathbb{R}^d$, $z \in \mathbb{R}^n$. Equation (1a) also takes into account the effect of an external potential $x \mapsto W(x)$. The system (1a)–(1b) is completed by initial data

$$\begin{aligned}&(q(0), \dot{q}(0)) = (q_0, p_0),\\ &(\psi(0, x, z), \partial_t\psi(0, x, z)) = (\psi_0(x, z), \psi_1(x, z)).\end{aligned} \tag{2}$$

A fundamental feature of the model is the conservation of the total energy. Let

$$E_{\text{particle}}(t) = \frac{1}{2}\dot{q}(t)^2 + W(q(t)) + \iint_{\mathbb{R}^d\times\mathbb{R}^n} \sigma_1(q(t) - y)\sigma_2(z)\psi(t, y, z)\,\mathrm{d}y\,\mathrm{d}z \tag{3}$$

*Corresponding author
thierry.goudon@inria.fr (T. Goudon); leo.vivion@unice.fr (L. Vivion)
ORCID(s):

and

$$E_{\rm wave}(t) = \frac{1}{2}\iint_{\mathbb{R}^d\times\mathbb{R}^n} \left|\partial_t\psi(t,x,z)\right|^2 \,\mathrm{d}x\,\mathrm{d}z + \frac{c^2}{2}\iint_{\mathbb{R}^d\times\mathbb{R}^n} \left|\nabla_z\psi(t,x,z)\right|^2 \,\mathrm{d}x\,\mathrm{d}z. \tag{4}$$

Then, we have

$$E(t) = E_{\rm particle}(t) + E_{\rm wave}(t) = E(0). \tag{5}$$

As time becomes large, the remarkable fact brought out in [5] is that the membranes eventually act as a friction force on the particle. To be more specific, the flavor of the large time asymptotics of the particle can be recapped in the following statement (for precise statements and detailed assumptions, we refer the reader to [5, Theorems 2 & 4]).

Theorem 1. *Let $n = 3$. For any $\eta \in (0,1)$ there exists a critical wave speed $c_0 = c_0(\eta) > 0$ and constants $\gamma, K > 0$ (which do not depend on η) such that the following assertions hold*

- Constant force, *[5, Theorem 2]: if $W(x) = \mathcal{F}\cdot x$ for a certain $\mathcal{F}\in\mathbb{R}^d$ constant and small enough compared to c^{-1}, then, there exists $q_\infty \in \mathbb{R}^d$ and $v(\mathcal{F})\in\mathbb{R}^d$ such that, for any $c \geq c_0$, we have*

$$\left|q_\infty + t\,v(\mathcal{F}) - q(t)\right| \leq K e^{-\frac{\gamma(1-\eta)}{c^3}t};$$

- Confining potential, *[5, Theorem 4]: if $W(x) \to_{|x|\to+\infty} +\infty$, then as time tends to ∞, $\dot q(t)$ converges to 0 and $q(t)$ converges to a critical point $q^\star$ of the potential W. If $q^\star$ is a non degenerate minimum of W, then, for any $c \geq c_0$, we have*

$$\left|q(t) - q^\star\right| \leq K e^{-\frac{\gamma(1-\eta)}{2c^3}t}.$$

Remark 2. *The following comments are worthwhile:*

- *We point out the role of the assumptions "the wave speed c is large enough" and on the dimension n for the wave propagation. That c is large can be interpreted as a condition ensuring that the energy is quickly evacuated in the membrane, when the particle hits this membrane. The following two intuitive arguments for choosing the dimension $n = 3$ can be given: first, it ensures a strong enough dispersion effect, which would be too weak in lower dimensions; second, the Huygens principle implies that the energy transferred to the membrane is really evacuated and cannot be felt at the hitting point after a while.*
- *When the particle is subjected to a constant external force, asymptotically as time becomes large it has a uniform rectilinear motion. Assuming $n = 3$ also allows us to identify the asymptotic action of the vibrations as a friction force proportional to the velocity of the particle (see [5, Eq. (2.9)]).*
- *When the particle is subjected to a confining potential, it stops exponentially fast at a critical point of the potential.*

This statement tells us that, in certain circumstances, the interaction with the environment acts on the particle as a drag force: the large time behavior looks like the one of the system

$$\dot q(t) = p(t), \qquad \dot p(t) = -\nabla W(q(t)) - \lambda p(t),$$

with an effective friction coefficient $\lambda > 0$. This is precisely the motivation presented in [5] to shed some light on the conditions driving to such a friction effect, by coming back to a more microscopic and detailed description of the interaction, that takes into account the dynamics of the environment, here represented by a scalar vibration field.

Therefore, this work fits in the framework of open systems theory where a classical, or quantum, system is coupled to its environment through exchanges of mass, momentum or energy. In turn, the environment has a dissipative action on the system, an idea that dates back to the seminal works of Caldeira-Leggett [6, 7]. We refer the reader to [27] for an overview on such models for classical particles, and the presentation of a quite general framework that encompasses many physical situations of interest. In particular, it is worth mentioning the related attempts to model frictional damping from the interaction with a wave field coupled to the moving particle [25, 26] and [19], where the environment is described as a Bose gas, and the slowing down of the particle is interpreted in terms of Cherenkov radiation effects. The originality of the model introduced in [5] is to model the environment as a vibrational field that can evacuate energy in directions transverse to the particle's motion. Then, the wish is to derive an effective formula, depending on the interaction parameters (here σ_1, σ_2, c...) for the drag coefficient λ. One also expects, for small applied force $\mathcal{F}$, that the limiting velocity $v(\mathcal{F})$ becomes proportional to the force: $v(\mathcal{F}) \sim_{\mathcal{F}\to 0} \mu\mathcal{F}$, in the spirit of Ohm's law, and one is interested in identifying the corresponding mobility μ. Complementary studies of the model (1a)–(1b) can be found in [1, 11, 12, 13, 27, 32], with connections to stochastic homogenization and to the classical Lorentz problems. We also refer to [8] for a quantum version of the model, and further connection to the Cherenkov radiation.

It is natural to extend the model (1a)–(1b) by considering a set of N particles which all interact with the membranes. Let q_i stand for the position of the ith particle. The system is now governed by the system

$$\ddot q_i(t) = -\nabla W(q_i(t)) - \iint_{\mathbb{R}^d\times\mathbb{R}^n} \sigma_1(q_i(t)-y)\sigma_2(z)\nabla_y\psi(t,y,z)\,\mathrm{d}y\,\mathrm{d}z,$$
$$\partial_{tt}^2\psi - c^2\Delta_z\psi = -\sigma_2(z)\left(\sum_{i=1}^N \sigma_1(x-q_i(t))\right),$$

for $t \geq 0$, $x\in\mathbb{R}^d$, $z\in\mathbb{R}^n$. Considering the mean field regime of this system (which amounts to deal with the limit

$N \to \infty$, assuming that the strength of the force on a given particle scales like $1/N$), one is led to a kinetic equation

$$\begin{aligned} &\partial_t F + v \cdot \nabla_x F \\ &- \nabla_x \left(W + \sigma_1 \star_x \int \sigma_2 \psi \, \mathrm{d}z \right) \cdot \nabla_v F = 0, \end{aligned} \tag{7a}$$

$$\partial_{tt}^2 \psi - c^2 \Delta_z \psi = -\sigma_2(z) \left(\sigma_1 \star_x \int F \, \mathrm{d}v \right), \tag{7b}$$

for $t \geq 0$, $x \in \mathbb{R}^d$, $v \in \mathbb{R}^d$, $z \in \mathbb{R}^n$, where the unknown F stands for the particles distribution function in phase space, see [21]. These systems still satisfy the energy conservation property (5), just adapting the definition of the energy associated to the particles as follows:

$$\begin{aligned} E_{\text{particles}}(t) = \sum_{i=1}^{N} \Big(&\frac{1}{2} \dot{q}_i(t)^2 + W(q_i(t)) \\ &+ \iint_{\mathbb{R}^d \times \mathbb{R}^n} \sigma_1(q_i(t) - y) \sigma_2(z) \psi(t, y, z) \, \mathrm{d}y \, \mathrm{d}z \Big) \end{aligned} \tag{8}$$

for (6a)–(6c) and

$$\begin{aligned} E_{\text{particles}}(t) = \iint_{\mathbb{R}^d \times \mathbb{R}^d} F(t, x, v) \Big(&\frac{v^2}{2} + W(x) \\ &+ \iint_{\mathbb{R}^d \times \mathbb{R}^n} \sigma_1(x - y) \sigma_2(z) \psi(t, y, z) \, \mathrm{d}y \, \mathrm{d}z \Big) \, \mathrm{d}x \, \mathrm{d}v \end{aligned} \tag{9}$$

for (7a)–(7b). We refer the reader to [9] for the well-posedness analysis of the Vlasov-Wave system (7a)–(7b). As a matter of fact, we point out that F naturally remains non-negative, all L^p ($1 \leq p \leq +\infty$) norms are conserved as well as the entropy functional

$$H(t) = \iint_{\mathbb{R}^d \times \mathbb{R}^d} F(t) \log(F(t)) \, \mathrm{d}x \, \mathrm{d}v.$$

More generally, for any $A : \mathbb{R}_+ \to \mathbb{R}$ the integral (Casimir functionals)

$$\iint_{\mathbb{R}^d \times \mathbb{R}^d} A(F(t)) \, \mathrm{d}x \, \mathrm{d}v$$

is conserved. These fundamental properties are consequences of the fact that the flow

$$\varphi_t : (x_0, v_0) \mapsto (\mathscr{X}(t), \mathscr{V}(t))$$

defined by the ODE system

$$\begin{aligned} &\frac{\mathrm{d}}{\mathrm{d}t} \mathscr{X}(t) = \mathscr{V}(t), \\ &\frac{\mathrm{d}}{\mathrm{d}t} \mathscr{V}(t) = -\nabla_x W(\mathscr{X}(t)) - \nabla_x \phi(t, \mathscr{X}(t)), \\ &\mathscr{X}(0) = x_0, \qquad \mathscr{V}(0) = v_0 \end{aligned} \tag{10}$$

where

$$\phi(t, x) = \iint_{\mathbb{R}^d \times \mathbb{R}^n} \sigma_1(x - y) \sigma_2(z) \psi(t, x, z) \, \mathrm{d}z \, \mathrm{d}y, \tag{11}$$

is symplectic. Indeed, denoting

$$J = \begin{pmatrix} 0_d & I_d \\ -I_d & 0_d \end{pmatrix},$$

we have

$$(\mathrm{Jac}\, \varphi_t)^T J (\mathrm{Jac}\, \varphi_t) = J.$$

In particular, $\det(\mathrm{Jac}\, \varphi_t)^2 = 1$ and volumes are conserved by the flow. We deduce the asserted conservation properties since the distribution function F is constant along the flow φ_t: for any $t \geq 0$, $F(t, x, v) = F_0(\varphi_{-t}(x, v))$.

Remark 3. *The construction of the numerical method will use this property, which equally applies to the particulate systems as follows. Given a solution of* (1a)–(1b)*, associated to the initial data* $(q_0, p_0, \Psi_0, \Psi_1)$*, we have at hand the potential defined by the formula* (11)*, and it makes sense to consider the differential system* (10) *(where a priori* $(x_0, v_0) \neq (q_0, p_0)$*; when the equality holds the trajectories coincide* $(q(t), p(t)) = (\mathscr{X}(t), \mathscr{V}(t))$*). It describes the motion of a "fictitious particle", governed by the potential* ϕ*. This system is still symplectic. A similar conclusion applies when starting from* (6a)–(6c)*. However, we warn the reader not to be confused: the differential system* (1a)–(1b)*, or* (6a)–(6c)*, itself is by no means symplectic (which would be contradictory with Theorem 1 and the numerical experiments). This observation will be crucial for the construction of the numerical scheme: on a given time step, one has to solve the ODE system with* ψ *considered as given, which motivates the use of a symplectic method in order to preserve accurately the energetic properties of the model.*

Remark 4. *Contrarily to a common practice, we have incorporated the interaction potential in definition* (3)*, and its counterparts for the many-particles frameworks. It is seen as the potential exerted by the wave on the particle, consistently with the viewpoint developed in [9]. This formulation will be also natural for discussing the numerical strategy and the preservation of the energy exchanges.*

One might wonder what the friction effect observed on a single particle becomes when one deals with a large number of particles, either with the discrete model (6a)–(6c) or the kinetic model (7a)–(7b). Surprisingly, the conclusion might substantially differ (see also the recent results in [35] which gives interesting hints on the large time behavior for the N particles system and comments on the loss of convergence rate in mean field regime $N \to \infty$). In fact the analysis performed in [9] establishes an unexpected connection between (7a)–(7b) and the *attractive* Vlasov–Poisson system, which can be obtained in a certain asymptotic regime as $c \to \infty$. In the same spirit, several stationary solutions of (7a)–(7b) can be identified, by means of free energy minimization, and their stability has been established [10]. Moreover, still based on the analogies with the Vlasov-Poisson system, it has been shown that the Vlasov-Wave system (7a)–(7b) can lead to a Landau damping effect, as summarized in the following statement (see [22] for further details).

Theorem 5. *Let $W = 0$, $n = 3$ and suppose that $x \in \mathbb{T}^d$. If the initial data (F_0, ψ_0, ψ_1) are homogeneous with respect to x, then the unique solution $(F(t), \psi(t))$ of (7a)–(7b) satisfies $F(t) = F_0$ for any t. If F_0 satisfies a certain criterion of linear stability and considering $(\widetilde{F}_0, \widetilde{\psi}_0, \widetilde{\psi}_1)$ small enough perturbations of (F_0, ψ_0, ψ_1), then, the associated solution $(\widetilde{F}(t), \widetilde{\psi}(t))$ of (7a)–(7b) satisfies the following properties:*

- *the force term*

$$-\nabla_x \left(\sigma_1 \star_x \int \sigma_2 \widetilde{\psi} \, \mathrm{d}z \right)$$

  converges (strongly) to 0,

- *if, moreover, $\widetilde{F}_0$ has the same mass as F_0, the macroscopic density $\int \widetilde{F} \, \mathrm{d}v$ converges (strongly) to $\int F_0 \, \mathrm{d}v$.*

Remark 6. *Let us make the following comments:*

- *The analysis follows arguments for the Vlasov-Poisson system, see [28] and [3]; it adapts also when dealing for the problem set on $\mathbb{R}^d$, following [4]. The decay rate can be explicited, depending on the functional framework for the perturbation $\widetilde{F}_0$.*

- *Given a spatially homogeneous profile F_0, the criterion ensuring the linear stability holds provided c is large enough.*

- *Again, the role of the dimension $n = 3$ (in fact n odd and $n \geq 3$) is crucial for establishing the Landau damping.*

We wish to investigate these questions on numerical grounds. In particular, we address the following issues:

- for the single particle model (1a)–(1b), to illustrate the validity of Theorem 1 and observe the friction effect, for both a confining potential or a constant force, in which case we discuss the behavior of the asymptotic speed.

- for (6a)–(6c), to investigate the N-particles large time dynamics. When $N > 1$ particles interact, the situation looks much more intricate and several scenario emerge. Roughly speaking either the particles ignore each other, possibly after a very short time of interaction, and they behave as they were alone, or they form clusters that create their own confining potential. Such cluster may move or stop, even if, individually, each particle in the cluster keeps moving. (Further results on the large time asymptotics for N particles in a confining potential can be found in [35].)

- For the kinetic model (7a)–(7b), to illustrate the Landau damping phenomena.

We will pay a specific attention to discuss the role of the assumptions of the wave-space dimension n, and on the wave-speed c. The numerical investigation of these questions require to take into consideration the specific features of the models in order to construct the numerical method:

- as said above, the friction/damping phenomena depend on the wave-space dimension n, and the case $n = 3$ definitely has a specific role. Moreover, these phenomena are, more or less, related to the ability to evacuate the energy through the membranes. Hence, one has to simulate the free space wave equation, in dimension $n = 3$. This requires to pay attention to the conditions imposed at the boundaries of the wave-computational domain, in order not to perturb the necessary dispersion effects, which are essential for the asymptotic properties.

- the energy balance, and in particular the exchanges between the kinetic energy of the particles and the vibrational energy of the membranes, are also crucial features of the models, and the discrete version of the problem should preserve as far as possible the dynamics of these exchanges.

These considerations will guide the technical choices to design the numerical scheme. The paper is organized as follows. In Section 2, we describe how we can take advantage of spherical symmetries to set up transparent boundary conditions for the wave equation in dimension $n = 3$. Sections 3 and 4 are devoted to the discretization of the equations, in the N particles and in the kinetic frameworks, respectively. In Section 5, we discuss in details the energetic properties of the schemes. We present the numerical results in Section 6.

2. Discretization of the wave equation with a transparent boundary condition

In dimension $n = 1$, the wave equation propagates the information to the right and to the left with velocities $\pm c$, and considering the expression of the solution given by D'Alembert's formula, we find that

$$(\partial_t + c\partial_x)\psi(t, R_{\max}) = 0 = (\partial_t - c\partial_x)\psi(t, -R_{\max})$$

constitues transparent boundary conditions that can be used when truncating the computational domain to the interval $(-R_{\max}, +R_{\max})$. Furthermore, these conditions can be easily implemented. Unfortunately, finding relevant boundary conditions in higher dimensions is far more challenging and leads to non local formula, see [14]. Nevertheless, in the particular case of the dimension $n = 3$ (note that Theorems 1 and 5 use this assumption) and for radially symmetric data, there exists a transformation that allows us to go back to the classical wave equation in dimension $n = 1$, see e.g. [36].

2.1. Radially symmetric wave equation

Consider the wave equation in dimension $n = 3$

$$\partial_{tt}^2 \psi - c^2 \Delta_z \psi = -\sigma_2(z) \, S(t, x). \tag{12}$$

We suppose that

$$\sigma_2(z) = \tilde{\sigma}_2(|z|)$$

is radially symmetric. If, furthermore, the initial condition

$$(\psi_0(x, z), \psi_1(x, z)) = (\Psi_0(x, |z|), \Psi_1(x, |z|))$$

is radially symmetric too, then the unique solution ψ of (12) is radially symmetric. We have $\psi(t,x,z) = \Psi(t,x,|z|)$ and Ψ satisfies

$$\partial_{tt}^2\Psi - c^2\left(\partial_{rr}^2\Psi + \frac{n-1}{r}\partial_r\Psi\right) = -\tilde{\sigma}_2(r)S(t,x).$$

We set

$$u(t,x,r) = r\Psi(t,x,r). \tag{13}$$

Using that $n = 3$, we check that u is a solution of the classical wave equation in dimension one

$$\partial_{tt}^2 u - c^2\partial_{rr}^2 u = r\left(\partial_{tt}^2\Psi - c^2\partial_{rr}^2\Psi - c^2\frac{2}{r}\partial_r\Psi\right) = -r\tilde{\sigma}_2(r)S(t,x).$$

Therefore, truncating the domain to $|z| \le R_{\max}$, we can use

$$\partial_t u + c\partial_r u = 0$$

as a (simple and exact) transparent boundary condition for $r = R_{\max}$. Eventually, we have to solve numerically the following system, for $t \ge 0$ and $0 < r < R_{\max}$,

$$\partial_{tt}^2 u - c^2\partial_{rr}^2 u = -r\tilde{\sigma}_2(r)S(t,x), \tag{14a}$$
$$(u(0,x,r), \partial_t u(0,x,r)) = (r\Psi_0(x,r), r\Psi_1(x,r)), \tag{14b}$$
$$u(t,x,0) = 0, \quad \partial_t u(t,x,R_{\max}) + c\partial_r u(t,x,R_{\max}) = 0. \tag{14c}$$

We remind the reader that x appears here as a parameter. In practice, we shall discretize the physical space, and thus we shall deal with this system for a finite number of grid points x. Once u determined by solving (14a)–(14c), we can come back to the original unknown Ψ (and then ψ): for any $r \neq 0$, we have $\Psi(t,x,r) = u(t,x,r)/r$ and for $r = 0$, we derive (13) to get

$$\partial_r u(t,x,r) = \Psi(t,x,r) + r\partial_r\Psi(t,x,r).$$

Since for any smooth solution of (12), $\partial_r\Psi(t,x,0)$ is bounded (in fact for these solutions $\partial_r\Psi(t,x,0) = 0$), we eventually get $\Psi(t,x,0) = \partial_r u(t,x,0)$. Nevertheless, for our purposes, it is not necessary to reconstruct ψ to solve (1a), (6a) or (7a). Indeed, for these three equations we can write the potential

$$\phi(t,x) = \iint_{\mathbb{R}^d\times\mathbb{R}^n} \sigma_1(x-y)\sigma_2(z)\psi(t,y,z)\,\mathrm{d}y\,\mathrm{d}z$$

by means of u:

$$\phi(t,x) = 4\pi\int_{\mathbb{R}^d}\sigma_1(x-y)\left(\int_0^{R_{\max}} r\tilde{\sigma}_2(r)u(t,y,r)\,\mathrm{d}r\right)\mathrm{d}y. \tag{15}$$

This equality (15) holds true as far as

$$\mathrm{supp}(\tilde{\sigma}_2) \subset [0, R_{\max}],$$

a condition that we shall use to choose the cut-off parameter $R_{\max}$.

2.2. Discretization of the radial wave equation (14a)–(14c).

Let us explain the discretization method for the wave equation; we use quite classical approaches and further information about the schemes can be found in e. g. [2, 37].

Radial discretization. We use a Finite Element Method (FEM). To this end, we introduce a subdivision

$$0 = r_1 < r_2 < .... < r_K = R_{\max}$$

of $[0, R_{\max}]$ and a basis $(\varphi_1, ..., \varphi_{\mathcal{K}_K})$ (with $\mathcal{K}_K \ge K$) of polynomial functions associated to this partition and the choice of the family of finite elements. The approached solution reads $u_h(t,x,r) = \sum_{k=1}^{\mathcal{K}_K} u_k(t,x)\varphi_k(r)$ where the numerical unknowns are collected in $U(t,x) = (u_1, ..., u_{\mathcal{K}_K})(t,x)$, the vector determined by the system

$$\mathcal{M}\frac{\mathrm{d}^2}{\mathrm{d}t^2}U(t,x) + \mathcal{C}\frac{\mathrm{d}}{\mathrm{d}t}U(t,x) + \mathcal{R}U(t,x) = G(t,x). \tag{16}$$

In (16), $\mathcal{M}$ is the mass matrix, $\mathcal{C}$ the diffusion matrix, $\mathcal{R}$ the rigidity matrix and the components of $G(t,x)$ are given by

$$-S(t,x)\int_0^{R_{\max}} r\tilde{\sigma}_2(r)\varphi_k(r)\,\mathrm{d}r, \qquad \text{for } k \in \{1, ..., \mathcal{K}_K\}.$$

Note that Dirichlet boundary conditions are encoded in the mass matrix $\mathcal{M}$ whereas the transparent boundary condition is encoded in the diffusion matrix $\mathcal{C}$.

Time discretization. Next, we make use of Newmark scheme for treating the time derivatives in (16). Let $\delta t > 0$ stand for the time step and set $t^n = n\delta t$. Then, the approximation of the solution u at time t^n is $u^n(x,r) = \sum_{k=1}^{\mathcal{K}_K} u_k^n(x)\varphi_k(r)$. We denote U_x^n the vector with components $u_k^n(x)$. For $G(t,x) = 0$, the Newmark scheme reads

$$\begin{aligned}&\mathcal{M}\frac{U_x^{n+1} - 2U_x^n + U_x^{n-1}}{\delta t^2}\\ &+ \mathcal{C}\frac{d\,U_x^{n+1} + (1-2d)U_x^n + (d-1)U_x^{n-1}}{\delta t}\\ &+ \mathcal{R}\left(\theta\,U_x^{n+1} + (1/2 + d - 2\theta)U_x^n\right.\\ &\qquad\left.+(1/2 - d + \theta)U_x^{n-1}\right) = 0\end{aligned} \tag{17}$$

where $0 \le d \le 1$ and $0 \le \theta \le 1/2$ are parameters of the scheme. Of course, in our situation, $G(t,x) \neq 0$ and the choice of the time discretization of G will depend on the coupling with (1a) (resp. (6a) or (7a)). This will be detailed later on. In practice we will only use this scheme with $(d,\theta) = (1/2, 1/4)$. For these parameters the scheme is second order accurate in time and kth order in space, where k depends of the choice of the FEM basis. Moreover, for these parameters, as far as the support of the wave remains included in the computational domain, the scheme conserves the discrete energy of the homogeneous wave equation. More precisely, as far as $\mathcal{C}U_x^m = 0$ for $m \in \{n-1, n, n+1\}$, we have

$$\left\langle \mathcal{M}\frac{U_x^{n+1}-U_x^n}{\Delta t/2}, \frac{U_x^{n+1}-U_x^n}{\Delta t/2} \right\rangle + \left\langle \mathcal{R}\frac{U_x^{n+1}+U_x^n}{2}, \frac{U_x^{n+1}+U_x^n}{2} \right\rangle = \left\langle \mathcal{M}\frac{U_x^n-U_x^{n-1}}{\Delta t/2}, \frac{U_x^n-U_x^{n-1}}{\Delta t/2} \right\rangle + \left\langle \mathcal{R}\frac{U_x^n+U_x^{n-1}}{2}, \frac{U_x^n+U_x^{n-1}}{2} \right\rangle. \quad (18)$$

3. Discretization of (1a)–(1b)

We restrict ourselves to the case where the particles evolve in the one-dimensional torus: $d = 1$ and $x \in \mathbb{T}_L := \mathbb{R}/(L\mathbb{Z})$ (where $L > 0$). For (1a), we thus impose $q(t) \in \mathbb{T}_L$. Then we are led to discretize the following system

$$\begin{cases} \dot{q}(t) = p(t), \\ \dot{p}(t) = -\partial_x W(q(t)) - \partial_x \phi(t, q(t)), \\ (q(0), \dot{q}(0)) = (q_0, p_0),\ q(t) \in \mathbb{T}_L, \end{cases}$$

coupled to

$$\begin{cases} \partial_{tt}^2 u - c^2 \partial_{rr}^2 u = -r\tilde{\sigma}_2(r)\sigma_1(x - q(t)), \\ (u(0, x, r), \partial_t u(0, x, r)) = (r\Psi_0(x, r), r\Psi_1(x, r)), \\ u(t, x, 0) = 0, \\ \partial_t u(t, x, R_{\max}) + c\partial_r u(t, x, R_{\max}) = 0, \end{cases}$$

where the potential ϕ is defined by (15).

As said in the previous section, we solve the wave equation with a classical Newmark scheme with parameters $(d, \theta) = (1/2, 1/4)$. This ensures second order accuracy in time, and kth order with respect to the wave direction (depending on the choice of the FEM; in practice we shall work with the Lagrange $\mathbb{P}_2$ elements, which reaches second order accuracy). The symplectic property of the flow is a fundamental feature of the model. Hence, we make use of the Stormer-Verlet scheme (see (23) below) which is a second order accurate symplectic scheme: the discrete flow $\varphi_n : (q_0, p_0) \mapsto (q^n, p^n)$ is symplectic, where q^n and p^n stand for the approximation of q and p at time t^n, respectively. Further details about symplectic schemes can be found e. g. in [20, Section 1.3.2] and [24, 31].

We are left with the question of handling the coupling between the two evolution equations. To this end, we pay attention to the energy exchanges. We have already introduced the subdivision $(r_1, ..., r_K)$ and the basis functions $(\varphi_1, ..., \varphi_{\mathcal{K}_k})$. Let $\Delta t > 0$ be the time step. We have set $t^n = n\Delta t$; we shall also need

$$t^{n+1/2} = (n + 1/2)\Delta t.$$

Next, we also define a subdivision of the physical domain

$$0 = x_1 < ... < x_i = i\Delta x < ... < x_N = L$$

characterized by the (uniform) space step Δx. We denote $[x_{i-\frac{1}{2}}, x_{i+\frac{1}{2}}]$ the cell centered at x_i. Therefore the numerical unknowns for the wave equation are denoted $u_{i,k}^n$; they define the following approximation u^n of the wave at time t^n

$$u^n(x, r) = \sum_{i=1}^{N}\sum_{k=1}^{\mathcal{K}_k} u_{i,k}^n \mathbf{1}_{\left[x_{i-\frac{1}{2}}, x_{i+\frac{1}{2}}\right]}(x)\varphi_k(r).$$

It is also convenient to introduce

$$u_k^n(x) = \sum_{i=1}^{N} u_{i,k}^n \mathbf{1}_{\left[x_{i-\frac{1}{2}}, x_{i+\frac{1}{2}}\right]}(x),$$

so that

$$u_{i,k}^n = \frac{1}{\Delta x}\int_{x_{i-\frac{1}{2}}}^{x_{i+\frac{1}{2}}} u_k^n(x)\,\mathrm{d}x.$$

We shall denote U_x^n and U_i^n the vector in $\mathbb{R}^{\mathcal{K}_K}$ with components $u_k^n(x)$ and $u_{i,k}^n$, respectively. Hence, the potential ϕ at time t^n can be approached by

$$\begin{aligned} \phi^n(x) &= 4\pi\int_0^L \sigma_1(x-y)\left(\int_0^{R_{\max}} r\tilde{\sigma}_2(r)u^n(y,r)\,\mathrm{d}r\right)\mathrm{d}y \\ &= 4\pi\sum_{i=1}^{N}\sum_{k=1}^{\mathcal{K}_K} u_{i,k}^n\left(\int_{x_{i-\frac{1}{2}}}^{x_{i+\frac{1}{2}}}\sigma_1(x-y)\,\mathrm{d}y\right) \\ &\qquad \times\left(\int_0^{R_{\max}} r\tilde{\sigma}_2(r)\varphi_k(r)\,\mathrm{d}r\right). \end{aligned} \quad (19)$$

Accordingly, we have

$$\begin{aligned} &(\partial_x\phi)^n(x) = \partial_x\phi^n(x) \\ &= 4\pi\sum_{i=1}^{N}\sum_{k=1}^{\mathcal{K}_K} u_{i,k}^n\left(\int_{x_{i-\frac{1}{2}}}^{x_{i+\frac{1}{2}}}\partial_x\sigma_1(x-y)\,\mathrm{d}y\right) \\ &\qquad\times\left(\int_0^{R_{\max}} r\tilde{\sigma}_2(r)\varphi_k(r)\,\mathrm{d}r\right) \\ &= 4\pi\sum_{i=1}^{N}\sum_{k=1}^{\mathcal{K}_K} u_{i,k}^n\left(-\sigma_1(x-x_{i+\frac{1}{2}}) + \sigma_1(x-x_{i-\frac{1}{2}})\right) \\ &\qquad\times\left(\int_0^{R_{\max}} r\tilde{\sigma}_2(r)\varphi_k(r)\,\mathrm{d}r\right). \end{aligned} \quad (20)$$

Having at hand the approximated quantity $u^{n+\frac{1}{2}}$, we define similarly the approached potential at time $t^{n+\frac{1}{2}}$. Eventually, we set

$$\phi^{n+\frac{1}{4}} = \frac{\phi^{n+\frac{1}{2}} + \phi^n}{2} \quad \text{et} \quad \partial_x\phi^{n+\frac{1}{4}} = \frac{\partial_x\phi^{n+\frac{1}{2}} + \partial_x\phi^n}{2}.$$

Time-discretization. Suppose that we have computed q^n, p^n, $u^{n-1/2}$ and u^n. We are going to update these quantities and define q^{n+1}, $p^{n+1/2}$, p^{n+1}, $u^{n+1/2}$ and u^{n+1}. To this end, we solve numerically the following two equations on the time interval $[t^n, t^{n+1}]$.

$$\begin{cases} \partial_{tt}^2 u - c^2 \partial_{rr}^2 u = -r\tilde{\sigma}_2(r)\,\sigma_1(x-q^n) \\ u(t^{n-\frac{1}{2}}) = u^{n-\frac{1}{2}}; u(t^n) = u^n \end{cases}$$

$$\begin{cases} \dot{q}(t) = p(t) \\ \dot{p}(t) = -\partial_x W(q(t)) - \partial_x \phi^{n+\frac{3}{4}}(q(t)) \\ q(t^n) = q^n; p(t^n) = p^n \end{cases}$$

The approximation q^n allows us to compute an approximation of the right hand side of the wave equation: $r\tilde{\sigma}_2(r)\sigma_1(x-q^n)$, that can be used on all the interval $[t^n, t^{n+1}]$. Then, we compute $u^{n+1/2}$ and u^{n+1} by applying the Newmark scheme on two half time steps. More precisely, we apply (17) with $\delta t = \Delta t/2$ and we average over the cell $(x_{i-1/2}, x_{i+1/2})$. It leads to the following scheme:

$$\begin{cases} \mathcal{M}\dfrac{U_i^{n+\frac{1}{2}} - 2U_i^n + U_i^{n-\frac{1}{2}}}{(\Delta t/2)^2} + \mathcal{C}\dfrac{U_i^{n+\frac{1}{2}} + U_i^{n-\frac{1}{2}}}{\Delta t/2} \\ \qquad + \mathcal{R}\left(\frac{1}{4}U_i^{n+\frac{1}{2}} + \frac{1}{2}U_i^n + \frac{1}{4}U_i^{n-\frac{1}{2}}\right) = G_i^n \\ \mathcal{M}\dfrac{U_i^{n+1} - 2U_i^{n+\frac{1}{2}} + U_i^n}{(\Delta t/2)^2} + \mathcal{C}\dfrac{U_i^{n+1} + U_i^n}{\Delta t/2} \\ \qquad + \mathcal{R}\left(\frac{1}{4}U_i^{n+1} + \frac{1}{2}U_i^{n+\frac{1}{2}} + \frac{1}{4}U_i^n\right) = G_i^n \end{cases} \tag{21}$$

where G_i^n stands for the vector in $\mathbb{R}^{\mathcal{K}_K}$ with components

$$-\left(\frac{1}{\Delta x}\int_{x_{i-\frac{1}{2}}}^{x_{i+\frac{1}{2}}} \sigma_1(x-q^n)\,\mathrm{d}x\right)\left(\int_0^{R_{\max}} r\tilde{\sigma}_2(r)\varphi_k(r)\,\mathrm{d}r\right). \tag{22}$$

We turn to the equation for the particle. With the obtained approximations of u, we define $\partial_x\phi^{n+1/2}$, $\partial_x\phi^{n+1}$ and $\partial_x\phi^{n+3/4} = (\partial_x\phi^{n+1/2} + \partial_x\phi^{n+1})/2$. Then we use on all the interval $[t^n, t^{n+1}]$ this approximation of the force term. Since the force term $-\partial_x W(x) - \partial_x\phi^{n+3/4}(x)$ is constant in time, applying the Stormer-Verlet scheme eventually leads to the following scheme:

$$\begin{cases} p^{n+\frac{1}{2}} = p^n - \dfrac{\Delta t}{2}\partial_x W(q^n) - \dfrac{\Delta t}{2}\partial_x\phi^{n+\frac{3}{4}}(q^n) \\ q^{n+1} = q^n + \Delta t\, p^{n+\frac{1}{2}} \\ p^{n+1} = p^{n+\frac{1}{2}} - \dfrac{\Delta t}{2}\partial_x W(q^{n+1}) - \dfrac{\Delta t}{2}\partial_x\phi^{n+\frac{3}{4}}(q^{n+1}). \end{cases} \tag{23}$$

The full scheme is obtained by combining (21) and (23). We will justify this time discretization in terms of energy balance in Section 5.

4. Discretization of (7a)–(7b)

Again, we restrict the discussion to the case $x \in \mathbb{T}_L$. Moreover we should also deal with a truncated velocity domain $[-V_{\max}, V_{\max}]$, where $V_{\max}$ is chosen large enough so that it is reasonable to impose

$$F(t, x, -V_{\max}) = 0 = F(t, x, V_{\max}),$$

considering initial data such that $\mathrm{supp}(F_0) \subset \mathbb{T}_L \times [-V_{\max}, V_{\max}]$. We are thus concerned with the simulation of (adding an external potential does not add any difficulty, and we take $W = 0$ in this presentation for the sake of clarity):

$$\begin{cases} \partial_t F + v\,\partial_x F - \partial_x\phi\,\partial_v F = 0 \\ F(0, x, v) = F_0(x, v) \\ F(t, 0, v) = F(t, L, v) \\ F(t, x, -V_{max}) = F(t, x, V_{max}) = 0 \end{cases}$$

$$\begin{cases} \partial_{tt}^2 u - c^2\partial_{rr}^2 u = -r\tilde{\sigma}_2(r)\sigma_1(x - q(t)) \\ (u(0, x, r), \partial_t u(0, x, r)) = (r\Psi_0(x, r), r\Psi_1(x, r)) \\ u(t, x, 0) = 0 \\ \partial_t u(t, x, R_{\max}) + c\partial_r u(t, x, R_{\max}) = 0 \end{cases}$$

where the potential ϕ is defined by (15).

The wave equation is treated by using the Newmark scheme and the FEM as described above. For the kinetic equation, we use a Semi-Lagrangian finite volume scheme: the Positive and Flux Conservative (PFC) method that guarantees at the discrete level the conservation of mass, positivity of the solution and a maximum principle. Details and comments about this scheme can be found e. g. in [18, 16, 17] and the references therein. Note that other approaches, based on DG or WENO approximations could be used as well, see [23, 29, 30] for details on such approaches for Vlasov's equations.

We adapt the time discretization described for (1a)–(1b) in order to care of the energy balance. With the time step $\Delta t > 0$ we still denote $t^n = n\Delta t$ and $t^{n+1/2} = (n+1/2)\Delta t$. We construct a grid of the phase space with space and velocity steps $\Delta x > 0$ and $\Delta v > 0$ respectively. Let $x_{i+1/2} = (i+1/2)\Delta x$, for $i \in \{1, ..., N\}$, and $v_{j+1/2} = (j+1/2)\Delta v$, for $j \in \{-M, ..., M\}$, with $N\Delta x = L$ and $M\Delta v = V_{\max}$. We denote by $C_{i,j}$ the cell $[x_{i-1/2}, x_{i+1/2}] \times [v_{j-1/2}, v_{j+1/2}]$, with center (x_i, v_j). From the discrete quantities $u_{i,k}^n$, we construct the approximation $(x, r) \mapsto u^n(x, r)$ as above. The potential ϕ^n and $\partial_x\phi^n$ are still defined by (19) and (20). From the numerical unknowns $F_{i,j}^n$, we define the approximated distribution function

$$F^n(x, v) = \sum_{i=1}^{N}\sum_{j=-M}^{M} F_{i,j}^n \mathbf{1}_{C_{i,j}}(x, v).$$

The macroscopic density ρ at time t^n is thus given by

$$\begin{aligned}\rho^n(x) &= \int_{-V_{max}}^{V_{max}} F_h(t,x,v)\,\mathrm{d}v \\ &= \sum_{i=1}^{N}\left(\Delta v \sum_{j=-M}^{M} F_{i,j}^n\right)\mathbf{1}_{\left[x_{i-\frac12},x_{i+\frac12}\right]}(x).\end{aligned} \tag{24}$$

The convolution $\sigma_1 \star \rho$ at time t^n becomes

$$\begin{aligned}(\sigma_1\star\rho)^n(x) &= \sigma_1\star\rho^n(x) \\ &= \Delta v\sum_{i=1}^{N}\sum_{j=-M}^{M} F_{i,j}^n\left(\int_{x_{i-\frac12}}^{x_{i+\frac12}}\sigma_1(x-y)\,\mathrm{d}y\right).\end{aligned} \tag{25}$$

4.1. Time-discretisation

Knowing the approximations of F and u up to t^n, we obtain the updated quantities $u^{n+1/2}$, u^{n+1} and F^{n+1} by solving the following equations on $[t^n, t^{n+1}]$:

$$\begin{cases}\partial_{tt}^2 u - c^2\partial_{rr}^2 u = -r\sigma_2(r)(\sigma_1\star\rho)^n,\\ u(t^{n-\frac12}) = u^{n-\frac12}\ ;\ u(t^n) = u^n,\end{cases}$$

$$\begin{cases}\partial_t F + v\,\partial_x F - \partial_x\phi^{n+\frac34}\,\partial_v F = 0.\\ F(t^n) = F^n\end{cases}$$

With F^n we determine $(\sigma_1\star\rho)^n$, which is used to evaluate the source term for the wave equation. Iterating over two time-steps $\delta t = \Delta t/2$ the Newmark scheme (17), we get $u^{n+1/2}$ and u^{n+1}. To be specific, we have

$$\begin{cases}\mathcal{M}\dfrac{U_i^{n+\frac12} - 2U_i^n + U_i^{n-\frac12}}{(\Delta t/2)^2} + \mathcal{C}\dfrac{U_i^{n+\frac12} + U_i^{n-\frac12}}{\Delta t/2}\\ \quad +\mathcal{R}\left(\frac14 U_i^{n+\frac12} + \frac12 U_i^n + \frac14 U_i^{n-\frac12}\right) = G_i^n\\ \\ \mathcal{M}\dfrac{U_i^{n+1} - 2U_i^{n+\frac12} + U_i^n}{(\Delta t/2)^2} + \mathcal{C}\dfrac{U_i^{n+1} + U_i^n}{\Delta t/2}\\ \quad +\mathcal{R}\left(\frac14 U_i^{n+1} + \frac12 U_i^{n+\frac12} + \frac14 U_i^n\right) = G_i^n\end{cases} \tag{26}$$

where $U_i^n = (u_{i,1}^n, ..., u_{i,\mathcal{K}_K}^n)$ and the components $G_{i,k}^n$ are defined by

$$-\left(\frac{1}{\Delta x}\int_{x_{i-\frac12}}^{x_{i+\frac12}}(\sigma_1\star\rho)^n(x)\,\mathrm{d}x\right)\left(\int_0^{R_{\max}} r\tilde{\sigma}_2(r)\varphi_k(r)\,\mathrm{d}r\right). \tag{27}$$

Having disposed of the wave equation, we compute the force terms $\partial_x\phi^{n+1/2}$ and $\partial_x\phi^{n+1}$, as well as

$$\partial_x\phi^{n+3/4} = \frac{\partial_x\phi^{n+1/2} + \partial_x\phi^{n+1}}{2}.$$

Replacing the force by this constant quantity over the time interval, we obtain F^{n+1} by solving the corresponding Liouville equation with the PFC scheme.

4.2. Discretisation of the kinetic equation with the PFC scheme

We start with the time-splitting

$$\begin{cases}\partial_t F^\star + v\,\partial_x F^\star = 0, \quad t\in[t^n,t^{n+1}]\\ F^\star(t^n) = F(t^n) = F^n\end{cases}$$

$$\begin{cases}\partial_t F^{\star\star} - \partial_x\phi^{n+\frac34}\,\partial_v F^{\star\star} = 0, \quad t\in[t^n,t^{n+1}]\\ F^{\star\star}(t^n) = F^\star(t^{n+1}).\end{cases}$$

The consistency analysis of such time splitting methods with Landau damping is considered in [15]. The solutions of these equations at the final time t^{n+1} are obtained by integrating along characteristics:

$$\begin{cases}F^\star(t^{n+1},x,v) &= F^\star(t^n, X(t^n,t^{n+1},x,v),v)\\ &= F^\star(t^n, x-\Delta t\,v, v),\\ F^{\star\star}(t^{n+1},x,v) &= F^{\star\star}(t^n,x,V(t^n,t^{n+1},x,v))\\ &= F^{\star\star}(t^n,x,v+\Delta t\,\partial_x\phi^{n+\frac34}(x)).\end{cases}$$

Let us set

$$F_{i,j}^{\star,n} = \frac{1}{\Delta x}\int_{x_{i-\frac12}}^{x_{i+\frac12}} F^\star(t^n,x,v_j)\,\mathrm{d}x,$$

and

$$F_{i,j}^{\star\star,n} = \frac{1}{\Delta v}\int_{v_{j-\frac12}}^{v_{j+\frac12}} F^{\star\star}(t^n,x_i,v)\,\mathrm{d}v.$$

On the one hand, we obtain

$$\begin{aligned}F_{i,j}^{\star,n+1} &= \frac{1}{\Delta x}\int_{x_{i-\frac12}-\Delta t\,v_j}^{x_{i-\frac12}} F^\star(t^n,x,v_j)\,\mathrm{d}x + F_{i,j}^{\star,n}\\ &\quad -\frac{1}{\Delta x}\int_{x_{i+\frac12}-\Delta t\,v_j}^{x_{i+\frac12}} F^\star(t^n,x,v_j)\,\mathrm{d}x,\end{aligned}$$

and, on the other hand, we get

$$\begin{aligned}F_{i,j}^{\star\star,n+1} &= \frac{1}{\Delta v}\int_{v_{j-\frac12}+\Delta t\,\partial_x\phi_i^{n+\frac34}}^{v_{j-\frac12}} F^{\star\star}(t^n,x_i,v)\,\mathrm{d}v\\ &+F_{i,j}^{\star\star,n} - \frac{1}{\Delta v}\int_{v_{j+\frac12}+\Delta t\,\partial_x\phi_i^{n+\frac34}}^{v_{j+\frac12}} F^{\star\star}(t^n,x_i,v)\,\mathrm{d}v,\end{aligned}$$

where we denote $\partial_x\phi_i^{n+3/4} = \partial_x\phi^{n+3/4}(x_i)$. The scheme relies on relevant approximations, denoted $\Psi_{i+1/2,j}^{\star,n}$ and $\Psi_{i,j+1/2}^{\star\star,n}$ respectively, of the integrals

$$\frac{1}{\Delta x}\int_{x_{i+\frac12}-\Delta t\,v_j}^{x_{i+\frac12}} F^\star(t^n,x,v_j)\,\mathrm{d}x$$

and

$$\frac{1}{\Delta v}\int_{v_{j+\frac12}+\Delta t\,\partial_x\phi_i^{n+\frac34}}^{v_{j+\frac12}} F^{\star\star}(t^n,x_i,v)\,\mathrm{d}v.$$

The scheme thus reads

$$\begin{cases} F_{i,j}^{\star,n} = F_{i,j}^{n} \\ F_{i,j}^{\star,n+1} = F_{i,j}^{\star,n} + \frac{1}{\Delta x}\left(\Psi_{i-1/2,j}^{\star,n} - \Psi_{i+1/2,j}^{\star,n}\right) \\ F_{i,j}^{\star\star,n} = F_{i,j}^{\star,n+1} \\ F_{i,j}^{\star\star,n+1} = F_{i,j}^{\star\star,n} + \frac{1}{\Delta v}\left(\Psi_{i,j-1/2}^{\star\star,n} - \Psi_{i,j+1/2}^{\star\star,n}\right) \\ F_{i,j}^{n+1} = F_{i,j}^{\star\star,n+1} \end{cases} \tag{28}$$

Definition of $\Psi_{i+1/2,j}^{\star,n}$ and $\Psi_{i,j+1/2}^{\star\star,n}$. We construct a polynomial approximation $F_h^n(x,v)$ of $F^n(x,v)$ by using the values $F_{i,j}^n$. Then, $\Psi_{i+1/2,j}^{\star,n}$ and $\Psi_{i,j+1/2}^{\star\star,n}$ are simply deduced by computing the primitive of the polynomial $F_h^n(x,v)$. In order to satisfy the fundamental properties of positivity, maximum principle and mass conservation, this reconstruction should incorporate slope limiters that control the effects of too high gradients, due in particular to filamentation effects in phase space. We refer the reader to [16, 17, 18, 33, 34] for further details on the pros and cons of the reconstruction techniques. Here, we make use of a reconstruction based on third order polynomials (thus third order accurate when the gradients remain moderate).

5. Discrete energy balance

In this Section, we motivate the construction of the scheme (21)–(23) and (26)–(28) by discussing the discrete energy balance. We point out that it could be misleading to conserve the discrete *total* energy. It is much more important to reproduce well the energy *exchanges* between the particles and the waves. Indeed, it might be possible to conserve exactly the total energy, but with particles and wave energies far from their expected values. For this reason, we focus our attention on the energy exchanges, possibly at the price of sacrificing the exact conservation of the total energy.

Let us go back to the basic energetic properties of the equations under consideration. If u is the solution of the wave equation

$$\partial_{tt}^2 u - c^2 \partial_{rr}^2 u = f,$$

then E_{wave} defined by (4) satisfies

$$\frac{\mathrm{d}}{\mathrm{d}t} E_{\text{wave}}(t) = \iint \partial_t u(t) f(t)\,\mathrm{d}x\,\mathrm{d}r,$$

and this energy is conserved when $f = 0$. If q is solution of the ODE

$$\ddot{q}(t) = -\nabla_x W(q(t)) - \nabla_x \phi(t, q(t)),$$

then E_{particle} defined by (3) satisfies

$$\frac{\mathrm{d}}{\mathrm{d}t} E_{\text{particle}}(t) = \big(\partial_t \phi\big)(t, q(t)).$$

In particular $E_{\text{particle}}(t)$ is conserved when the potential ϕ does not depend on the time variable. Going back to the coupled system (1a)–(1b), the total energy $E = E_{\text{wave}} + E_{\text{particle}}$ is conserved because the source term f of the wave equation and the time-dependent potential ϕ fulfil the cancellation property

$$\iint \partial_t u(t) f(t)\,\mathrm{d}x\,\mathrm{d}r + \partial_t \phi(t, q(t)) = 0.$$

Therefore, the guidelines for constructing a energetically relevant scheme for (1a)–(1b) should be:

(*i*) the scheme for the wave equation conserves the discrete analog of E_{wave} when the source term f vanishes,

(*ii*) the scheme for the particle equation conserves the discrete analog of E_{particle} when the potential ϕ does not depend on time,

(*iii*) the discrete coupling is such that the contributions from the analog of $\iint \partial_t u(t) f(t)\,\mathrm{d}x\,\mathrm{d}r$ and $\partial_t \phi(t, q(t))$ cancel out.

Criterion (*i*) is a standard requirement for a scheme for the wave equation; by the way it is fulfilled by (21). Item (*ii*) is more delicate; having a symplectic scheme usually guarantees it is satisfied approximately, the discrete energy oscillates about the expected value, and energy conservation holds only in average. The coupling strategy devised above, see (21)–(23), is precisely intended to satisfy (*iii*). The constructed scheme is satisfactory in this sense: the energy echange is exactly treated and the error on the total energy is controlled by the error produced by the symplectic scheme designed for a hamiltonian system.

We follow the same reasoning for the system (7a)–(7b). We are dealing with a kinetic equation

$$\partial_t F + v \cdot \nabla_x F - \nabla_x \phi(t) \cdot \nabla_v F = 0$$

and the energy $E_{\text{particles}}$ defined by (9) satisfies

$$\frac{\mathrm{d}}{\mathrm{d}t} E_{\text{particles}}(t) = \iint F(t) \partial_t \phi(t)\,\mathrm{d}x\,\mathrm{d}v.$$

Like for the ODE describing a single particle, when the potential ϕ does not depend on the time variable, the energy $E_{\text{particles}}$ is conserved. Going back to the coupled system (7a)–(7b), the conservation of $E = E_{\text{wave}} + E_{\text{particles}}$ relies on the cancellation of the coupling terms

$$\iint \partial_t u(t) f(t)\,\mathrm{d}x\,\mathrm{d}r + \iint F(t) \partial_t \phi(t)\,\mathrm{d}x\,\mathrm{d}v = 0.$$

Therefore, the numerical strategy is based on the following requirements

(*i*) the scheme for the wave equation conserves the discrete analog of E_{wave} when the source term f vanishes,

(*ii*) the scheme for the kinetic equation conserves the discrete analog $E_{\text{particles}}$ when the potential ϕ does not depend on time,

(*iii*) the discrete coupling is such that the contributions from the analog of $\iint \partial_t u(t) f(t)\,\mathrm{d}x\,\mathrm{d}r$ and $\iint F(t)\partial_t\phi(t)\,\mathrm{d}x\,\mathrm{d}v$ cancel out.

Again, (*ii*) is not exactly satisfied by the discretization techniques, which, nevertheless, conserve positivity, L^1 and L^∞ estimates. The coupling requirement (*iii*) is specifically addressed by (26)–(28): the energy exchange is exactly handled by the scheme, and the error on the total energy is controlled by the error made on the Vlasov equation.

Let us now explain how (*iii*) is satisfied by the scheme (21)–(23) and (26)–(28).

5.1. The one-particle model

Let D be the operator which associates to a real valued sequence $(a^n)_{n\in\mathbb{N}}$ the finite difference sequence defined by

$$(Da^n) = (a^{n+1} - a^n).$$

We remind the reader that $u^{n-1/2}$ and u^n come from (21), $\phi^{n-1/2}$ and ϕ^n are defined by (19), and we have set $\phi^{n-1/4} = (\phi^{n-1/2} + \phi^n)/2$. We also set

$$u^{n-1/4} = \frac{u^n + u^{n-1/2}}{2} \quad \text{and} \quad \partial_t u^{n-1/4} = \frac{u^n - u^{n-1/2}}{\Delta t/2}.$$

We define the following discrete energies at time t^n:

$$E^n_{\text{wave}} = 4\pi \iint \frac{1}{2}\left|\partial_t u^{n-\frac14}(x,r)\right|^2 + \frac{c^2}{2}\left|\partial_r u^{n-\frac14}(x,r)\right|^2 \mathrm{d}x\,\mathrm{d}r,$$

and

$$E^n_{\text{particle}} = \frac{1}{2}(p^n)^2 + W(q^n) + \phi^{n-\frac14}(q^n).$$

Observe that

$$\begin{aligned} E^n_{\text{wave}} &= 2\pi\Delta x \sum_{i=1}^N \left\langle \mathcal{M}\tfrac{U_i^n - U_i^{n-\frac12}}{\Delta t/2}, \tfrac{U_i^n - U_i^{n-\frac12}}{\Delta t/2}\right\rangle \\ &\quad + 2\pi\Delta x \sum_{i=1}^N \left\langle \mathcal{R}\tfrac{U_i^n + U_i^{n-\frac12}}{2}, \tfrac{U_i^n + U_i^{n-\frac12}}{2}\right\rangle. \end{aligned}$$

Owing to (18), we get

$$D\,E^n_{\text{wave}} = 2\pi\Delta x \sum_{i=1}^N \left\langle G_i^n, D\,U_i^n + D\,U_i^{n-\frac12}\right\rangle,$$

where G_i^n is given by (22). Next, we have

$$\begin{aligned} D\,E^n_{\text{particle}} &= \frac{1}{2}(p^{n+1})^2 + W(q^{n+1}) + \phi^{n-\frac34}(q^{n+1}) \\ &\quad - \left[\tfrac{1}{2}(p^n)^2 + W(q^n) + \phi^{n-\frac34}(q^n)\right] \\ &\quad + D\,\phi^{n-\frac14}(q^n). \end{aligned}$$

We arrive at the following claim.

Theorem 7. *The scheme (21)–(23) is consistent for the energy exchange, which means that, for any $n \in \mathbb{N}$,*

$$2\pi\Delta x \sum_{i=1}^N \left\langle G_i^n, D\,U_i^n + D\,U_i^{n-\frac12}\right\rangle + D\,\phi^{n-\frac14}(q^n) = 0.$$

Let $E^n = E^n_{\text{wave}} + E^n_{\text{particle}}$. We have

$$\begin{aligned} D\,E^n &= \frac{1}{2}(p^{n+1})^2 + W(q^{n+1}) + \phi^{n-\frac34}(q^{n+1}) \\ &\quad - \left[\tfrac{1}{2}(p^n)^2 + W(q^n) + \phi^{n-\frac34}(q^n)\right]. \end{aligned} \tag{29}$$

This statement means that the error on the total discrete energy corresponds exactly to the error made on E_{particle} by the symplectic scheme. Note that (29) holds as far as (18) is satisfied, which itself relies on the assumption that the wave has not crossed the boundary of the computational domain (this is expressed through the assumption that $CU_x^m = 0$ for $m \in \{n-1, n, n+1\}$). This is not an issue since the energy that leaves the computational domain can be explicitely computed and incorporated in the energy balance.

Proof. On the one hand, we have

$$\begin{aligned} &2\pi\Delta x \sum_{i=1}^N \left\langle G_i^n, D\,U_i^n + D\,U_i^{n-\frac12}\right\rangle \\ &= 2\pi\Delta x \sum_{i=1}^N \sum_{k=1}^{\mathcal{K}_K} G_{i,k}^n \left[(u_{i,k}^{n+1} - u_{i,k}^n) + (u_{i,k}^{n+\frac12} - u_{i,k}^{n-\frac12})\right] \\ &= -2\pi \sum_{i=1}^N \sum_{k=1}^{\mathcal{K}_K} \left(\int_{x_{i-\frac12}}^{x_{i+\frac12}} \sigma_1(x - q^n)\,\mathrm{d}x\right) \\ &\qquad \times \left(\int_0^{R_{\max}} r\tilde{\sigma}_2(r)\varphi_k(r)\,\mathrm{d}r\right) \\ &\qquad\qquad \times \left[(u_{i,k}^{n+1} - u_{i,k}^n) + (u_{i,k}^{n+\frac12} - u_{i,k}^{n-\frac12})\right]. \end{aligned}$$

On the other hand, we get

$$\begin{aligned} D\,\phi^{n-\frac14}(q^n) &= 2\pi \sum_{i=1}^N \sum_{k=1}^{\mathcal{K}_K} Du_{i,k}^{n-\frac14} \left(\int_{x_{i-\frac12}}^{x_{i+\frac12}} \sigma_1(q^n - x)\,\mathrm{d}x\right) \\ &\quad \times \left(\int_0^{R_{\max}} r\tilde{\sigma}_2(r)\varphi_k(r)\,\mathrm{d}r\right) \\ &= 2\pi \sum_{i=1}^N \sum_{k=1}^{\mathcal{K}_K} \left(\int_{x_{i-\frac12}}^{x_{i+\frac12}} \sigma_1(q^n - x)\,\mathrm{d}x\right) \\ &\quad \times \left(\int_0^{R_{\max}} r\tilde{\sigma}_2(r)\varphi_k(r)\,\mathrm{d}r\right) \\ &\qquad \times \left[(u_{i,k}^{n+1} - u_{i,k}^n) + (u_{i,k}^{n+\frac12} - u_{i,k}^{n-\frac12})\right]. \end{aligned}$$

That the two quantities compensate is a consequence of the fact that σ_1 is even. This ends the proof. ∎

5.2. The kinetic model

The relation

$$D\,E^n_{\rm wave} = 2\pi\Delta x \sum_{i=1}^{N} \left\langle G_i^n, D\,U_i^n + D\,U_i^{n-\frac12} \right\rangle,$$

still holds, with now G_i^n defined in (27). With F^n given by (28) we set

$$E^n_{\rm particles} = \iint F^n(x,v)\left(\frac{v^2}{2} + \phi^{n-\frac14}(x)\right) \mathrm{d}x\,\mathrm{d}v.$$

We obtain

$$\begin{aligned} D\,E^n_{\rm particles} &= \iint D\,F^n(x,v)\left(\frac{v^2}{2} + \phi^{n-\frac14}(x)\right) \mathrm{d}x\,\mathrm{d}v \\ &\quad + \iint F^n(x,v) D\,\phi^{n-\frac14}(x)\,\mathrm{d}x\,\mathrm{d}v. \end{aligned}$$

Theorem 8. *The scheme (26)–(28) is consistent for the energy exchange, which means that, for any $n \in \mathbb{N}$,*

$$\begin{aligned} &2\pi\Delta x \sum_{i=1}^{N} \left\langle G_i^n, D\,U_i^n + D\,U_i^{n-\frac12} \right\rangle \\ &+ \iint F^n(x,v) D\,\phi^{n-\frac14}(x)\,\mathrm{d}x\,\mathrm{d}v = 0. \end{aligned}$$

Let $E^n = E^n_{\rm wave} + E^n_{\rm particles}$. We have

$$\begin{aligned} D\,E^n &= D\,E^n_{wave} + D\,E^n_{density} \\ &= \iint D\,F^n(x,v)\left(\frac{v^2}{2} + \phi^{n-\frac14}(x)\right) \mathrm{d}x\,\mathrm{d}v. \end{aligned}$$

As a consequence, the error on the total energy only comes from the error on the particles kinetic energy, as produced by the Semi-Lagrangian method (or the alternative method that could be used for the Vlasov equation).

Proof. We have

$$\begin{aligned} &2\pi\Delta x \sum_{i=1}^{N} \left\langle G_i^n, D\,U_i^n + D\,U_i^{n-\frac12} \right\rangle \\ &= 2\pi\Delta x \sum_{i=1}^{N}\sum_{k=1}^{\mathcal{K}_K} G^n_{i,k}\left[(u^{n+1}_{i,k} - u^n_{i,k}) + (u^{n+\frac12}_{i,k} - u^{n-\frac12}_{i,k})\right] \\ &= -2\pi \sum_{i=1}^{N}\sum_{k=1}^{\mathcal{K}_K}\left(\int_{x_{i-\frac12}}^{x_{i+\frac12}} \sigma_1 \star \rho^n(x)\,\mathrm{d}x\right) \\ &\quad\times\left(\int_0^{R_{\max}} r\tilde\sigma_2(r)\varphi_k(r)\,\mathrm{d}r\right) \\ &\qquad\times\left[(u^{n+1}_{i,k} - u^n_{i,k}) + (u^{n+\frac12}_{i,k} - u^{n-\frac12}_{i,k})\right] \end{aligned}$$

with $\sigma \star \rho^n$ defined in (25). It recasts as

$$\begin{aligned} &2\pi\Delta x \sum_{i=1}^{N} \left\langle G_i^n, D\,U_i^n + D\,U_i^{n-\frac12} \right\rangle \\ &= -2\pi\Delta v \sum_{i=1}^{N}\sum_{k=1}^{\mathcal{K}_K}\sum_{i'=1}^{N}\sum_{j=-M}^{M} F^n_{i',j} \\ &\quad\times\left(\int_{x_{i-\frac12}}^{x_{i+\frac12}}\int_{x_{i'-\frac12}}^{x_{i'+\frac12}} \sigma_1(x-y)\,\mathrm{d}x\,\mathrm{d}y\right) \\ &\quad\times\left(\int_0^{R_{\max}} r\tilde\sigma_2(r)\varphi_k(r)\,\mathrm{d}r\right) \\ &\qquad\times\left[(u^{n+1}_{i,k} - u^n_{i,k}) + (u^{n+\frac12}_{i,k} - u^{n-\frac12}_{i,k})\right]. \end{aligned}$$

Next, we have

$$\begin{aligned} &\iint F^n(x,v) D\,\phi^{n-\frac14}(x)\,\mathrm{d}x\,\mathrm{d}v \\ &= \Delta v \sum_{i=1}^{N}\sum_{j=-M}^{M} F^n_{i,j}\left(\int_{x_{i-\frac12}}^{x_{i+\frac12}} D\,\phi^{n-\frac14}(x)\,\mathrm{d}x\right) \\ &= 4\pi\Delta v \sum_{i=1}^{N}\sum_{j=-M}^{M}\sum_{i'=1}^{N}\sum_{k=1}^{\mathcal{K}_K} F^n_{i,j}\,Du^{n-\frac14}_{i',k} \\ &\quad\times\left(\int_{x_{i-\frac12}}^{x_{i+\frac12}}\int_{x_{i'-\frac12}}^{x_{i'+\frac12}} \sigma_1(x-y)\,\mathrm{d}x\,\mathrm{d}y\right) \\ &\quad\times\left(\int_0^{R_{\max}} r\tilde\sigma_2(r)\varphi_k(r)\,\mathrm{d}r\right) \\ &= 2\pi\Delta v \sum_{i=1}^{N}\sum_{j=-M}^{M}\sum_{i'=1}^{N}\sum_{k=1}^{\mathcal{K}_K} F^n_{i,j} \\ &\quad\times\left(\int_{x_{i-\frac12}}^{x_{i+\frac12}}\int_{x_{i'-\frac12}}^{x_{i'+\frac12}} \sigma_1(x-y)\,\mathrm{d}x\,\mathrm{d}y\right) \\ &\quad\times\left(\int_0^{R_{\max}} r\tilde\sigma_2(r)\varphi_k(r)\,\mathrm{d}r\right) \\ &\qquad\times\left[(u^{n+1}_{i',k} - u^n_{i',k}) + (u^{n+\frac12}_{i',k} - u^{n-\frac12}_{i',k})\right]. \end{aligned}$$

Again, since σ_1 is even, the two quantities compensate, which concludes the proof.

Like for the one-particle model, the statement holds as far as (18) holds. Otherwise, the energy which goes away the computational domain for the wave equation should be taken into account in the energy balance. ∎

6. Numerical results

In this Section we perform several numerical simulations. Our purpose is two-fold: on the one hand, we check the ability of the scheme in reproducing the expected behavior of the system as asserted in Theorems 1 and 5, in particular concerning the energy exchanges, and in capturing the rate of convergence; on the other hand, we also discuss the physical effects and the role of the assumptions in Theorems 1 and 5. We consider the following situations:

- *Single particle.* We wish to illustrate the statements in Theorem 1: the particle stops at the critical point of a confining potential; in the free-force case, the particle slows down due to the interaction with the environment; with a constant force, the particle asymptotically moves at a constant speed, that depends linearly on the applied force. These findings however assumes that the wave speed c is large enough; we shall see on numerical grounds that the behavior is indeed different from the conclusions of Theorem 1 when c is small.
- *N-particles.* The theory is far less advanced for this situation, which leads to quite intricate indirect interactions between the particles. The simulations reveal that several scenario can occur and they provide ground for conjectures about the stability of specific states.
- *Kinetic model.* We wish to illustrate the statements in Theorem 5. In particular, the proof of the Landau damping requires a stability condition which involves the wave speed c and the spreading of the initial condition. We shall discuss on numerical grounds the effects of these conditions. We will also briefly show that the dimension n of the vibrational space is crucial; in particular the damping does not hold when $n = 1$.

For all the simulations discussed below, we work with the compactly supported form functions:

$$\sigma_1(x) = \exp\Big(-\frac{1}{\epsilon^2 - x^2}\Big)\mathbf{1}_{-\epsilon\le x\le\epsilon},$$

and

$$\sigma_2(z) = \tilde\sigma_2(|z|), \qquad \tilde\sigma_2(r) = \exp\Big(-\frac{1}{R^2 - r^2}\Big)\mathbf{1}_{0\le r\le R}.$$

Of course, the shape of the solutions is influenced by σ_1, σ_2. In particular it changes the depth and the width of the potential wells, but the general features are well represented with these functions. The regularity of σ_1 is quite important in the analysis of the equations, but it is not clear in the experiments the dealing with less regular form functions has a significant role. The simulations are performed on the slab $(-L, L)$, with periodic boundary conditions. For the Vlasov case, the initial data for the particle distribution function is given by

$$F_0(x, v) = Z\Big(1 + a\cos\Big(\frac{2\pi}{L}x\Big)\Big)\exp(-v^2/2),$$

with $a > 0$ and Z the normalizing constant (so that F_0 is normalized: $\iint F_0\,\mathrm{d}v\,\mathrm{d}x = 1$). For the wave equation, we simply set $(\Psi_0, \Psi_1) = 0$.

For the particle simulations, the initial data for the wave equation is given by $\Psi_1 = 0$ and Ψ_0 solution of the stationary equation $-c^2\Delta_z\Psi_0(z) = -\sigma_2(z)\sigma_1(x - q_0)$, with q_0 the initial data of the particle. This quantity is determined numerically by working with the radial coordinate $r = |z|$, and by using a suitable approximation of stationary solutions based on infinite elements.

Table 1 collects the parameters used in the simulations. The other parameters depend on the considered situation.

Table 1
General data for the numerical simulations

ϵ	R	$R_{\max}$	a	$V_{\max}$
1	1	$2R$	.1	7

Table 2
Data for the simulations with a confining potential

$W(x)$	c	T	L	Δt	Δx	Δr
$.3x^2$	.5	40	3	2.10^{-2}	3/128	2/128

6.1. Simulations for a single particle

Confining potential. We start with the case of the confining potential in (1a)–(1b). We have used the data collected in Table 2. The simulations illustrate the second item of Theorem 1: the particle is trapped by the bottom of the well of the confining potential. It goes back and forth and slows down in the well of the potential. The phase portraits depicted in Fig. 2 with different initial data illustrate this effect. Fig. 2 also shows the evolution of the total energy and of the energy balance. On the one hand, the total energy is not exactly preserved, but the error remains of order 10^{-4} on the time scale of observation, thus confirming the robustness of the scheme. Similar observations apply to all the simulations. On the other hand, for the energy balance, we observe that the particle looses its kinetic energy, which is gained by the membranes. We warn the reader that with the adopted definition (3), E_{particle} contains asymptotically only the interaction energy, since the kinetic energy of the particle and the energy associated to the external potential tend to 0. Fig. 3 illustrates the role of the wave speed c: while the velocity of the particle clearly tends to 0 (exponentially fast, Fig. 3-left) when c is large, the damping is less visible with small c's on Fig. 3-right.

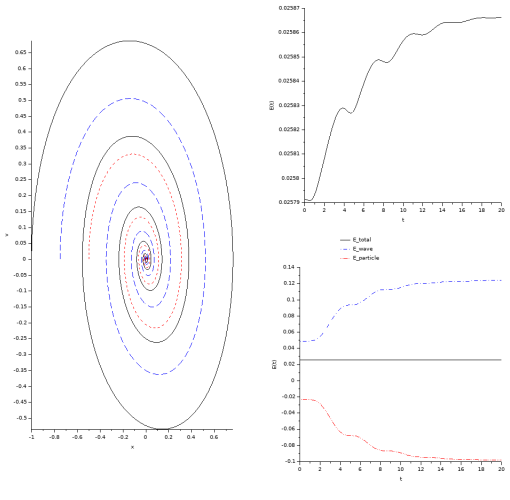

Figure 2: Single particle with a confining potential (Table 2): phase portrait (left) and evolution of the energy (right)

No external force. Next, we consider the case where there

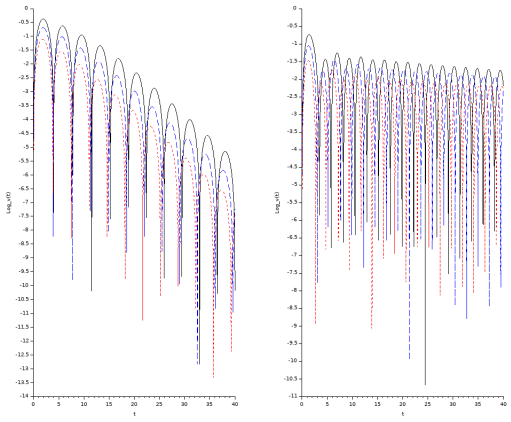

Figure 3: Single particle with a confining potential (Table 2): evolution of the particle velocity for several initial data (left: $c = .5$, right $c = .25$)

is no external force. The data for these simulations are collected in Table 3.

We start with the situation where c is large enough (Test 1). The interaction with the waves acts as a drag on the particle, which makes it slow down. Note on the figure that the well of the potential created by the vibrating field is slightly delayed compared to the position of the particle, see Fig. 4.

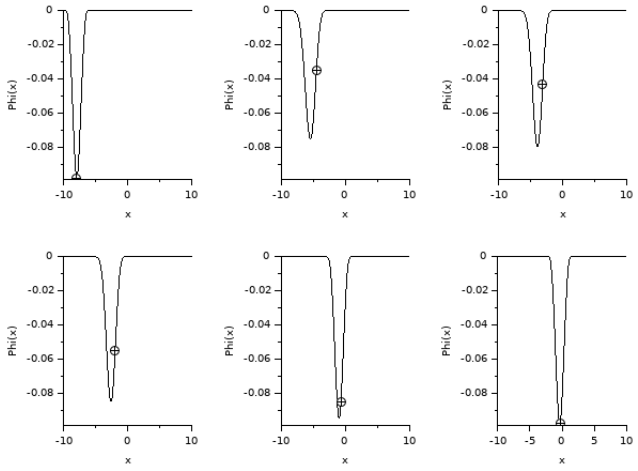

Figure 4: Single particle without external force (Table 3): delay between the particle position and the potential created by the vibrating field

It can be observed that the larger c, the smaller the delay. (More precisely, the leading quantity is the ratio $c/\dot{q}(0)$.) For such large c's, the particle eventually stops, as announced in [5], see Theorem 1: this is illustrated by the phase portraits and the velocity evolution in Fig. 5. However, when c is smaller (Test 2), we observe oscillations: the position of the well of the self-consistent potential oscillates, and the particle itself oscillates in the well of this potential. The phase portrait contrasts significantly with the case where c is large, exhibiting spirals, instead of a neat stop, see Fig. 6. It is difficult to predict whether this situation leads to a limit cycle or a full stop; anyway if the latter occurs it would be with a far smaller rate.

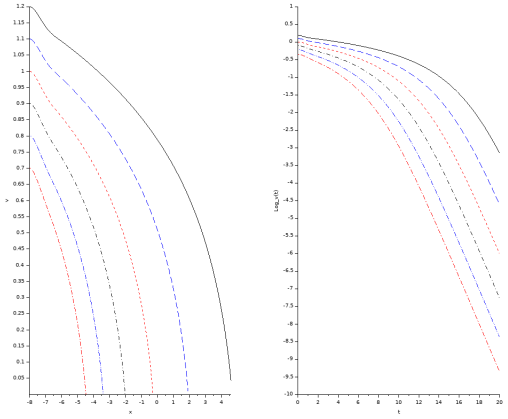

Figure 5: Single particle without external force (Table 3): phase portrait (left) and velocity evolution (right) for Test 1 (c large), for several initial data

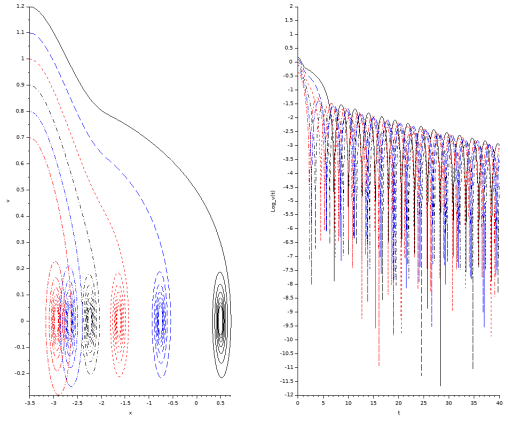

Figure 6: Single particle without external force (Table 3): phase portrait (left) and velocity evolution (right) for Test 2 (c small), for several initial data

Constant force. Finally, we deal with the case of a constant external force, which is specifically studied in [5], see the first item in Theorem 1. The data for these simulations are given in Table 4.

Table 3
Data for the force-free simulations

	$W(x)$	c	T	L	Δt	Δx	Δr
Test 1	0	.5	20	20	2.10^{-2}	20/512	2/128
Test 2	0	.25	20	10	2.10^{-2}	10/256	2/128

Table 4
Data for the simulation with a constant force

	$\mathcal{F}$	c	T	L	Δt	Δx	Δr
Test 1	-.1	.5	40	20	2.10^{-2}	20/512	2/128
Test 2	-.065	.5	40	10	2.10^{-2}	10/256	2/128

We start with the situation where the strength of $\mathcal{F}$ is not small enough compared to $1/c$ (Test 1); the statement in Theorem 1 does not apply. This is indeed what we observe in the simulation: the damping effect is too weak and the speed of the particle keeps growing (see Fig. 7-bottom-left). For the same value of c, we choose a smaller value of $\mathcal{F}$ (Test 2), so that the conditions of Theorem 1 are satisfied. We see in Fig. 7-top-right that the well of the potential is deeper (see Remark 9 below), and the damping effect exerted by the wave is indeed stronger. We clearly observe on Fig. 7-bottom-right that the speed of the particle tends to a limit value, and for large times the particle has a rectilinear motion with this speed. We perform the same simulation by making the applied force $\mathcal{F}$ vary: the behavior of the asymptotic speed $v(\mathcal{F})$ is depicted in Fig. 8, where the expected linear behavior can be observed for small $\mathcal{F}$'s, with a slope $\simeq 2.6$.

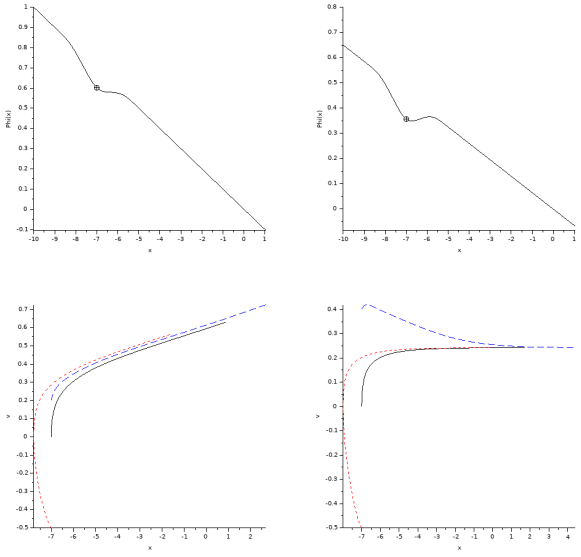

Figure 7: Left: Single particle with a constant force $\mathcal{F}$ not small enough compared to $1/c$ (Table 4, Test 1). Right: Single particle with a constant force $\mathcal{F}$ small enough compared to $1/c$ (Table 4, Test 2) Top: self-consistent potential at a certain time, and position of the particle; bottom: phase portrait for several initial data

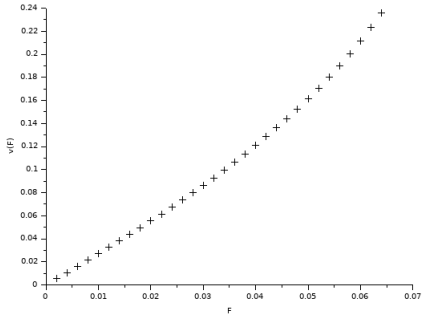

Figure 8: Asymptotic speed versus strength of the external force (Table 4, Test 2)

Remark 9. *It makes sense to rescale the equations so that the coupling term in the wave equation behaves like c^2. This is the scaling adopted in [9] in order to derive from (7a)–(7b) an attractive Vlasov equation. This scaling might be also motivated by the following considerations. With this rescaling the damping rate in Theorem 1 behaves like $1/c$ instead of $1/c^3$. If we work with this rescaled version of the equation, the depth of the potential remains unchanged by making c vary, but the faster evacuation of the energy through the membranes reduces the delay between particle's and potential well positions. With this re-scaling, the smallness condition on the force $\mathcal{F}$ becomes uniform with respect to c.*

6.2. Simulations for N particles

When dealing with $N > 1$ particles, see (6a)–(6c), few rigorous results are known and the asymptotic behavior of the system is certainly quite involved. When the particles are subjected to a confining potential, we observe that they are all just trapped in the well of the potential, and we can infer from the analysis in [35] that they eventually stop in the bottom of that well. However, the statements in [35] involve technical assumptions on the form functions which are not easy to check in practice, and the proof relies on compactness arguments that do not provide any convergence rate, which likely depends, at least, on the number of particles. Fig. 9 and Fig. 10 present the results of simulations with 2 particles. A remarkable observation is that the two particles

seem to self-organize in opposition of phase. The mean velocity tends to 0, exponentially fast (see Fig. 11), but it is not clear at all that the individual velocities vanish for large time, see in particular Fig. 10. At least, the observed rate of convergence is not exponential and it can become very slow, see Fig. 9 and Fig. 10, compared to Fig. 3. The data for this simulation are collected in Table 5.

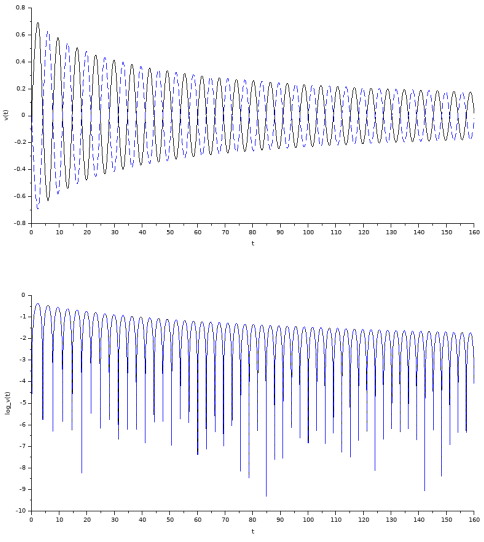

Figure 9: Two particles in a confining potential, evolution of the velocities I (Table 5-Test 1)

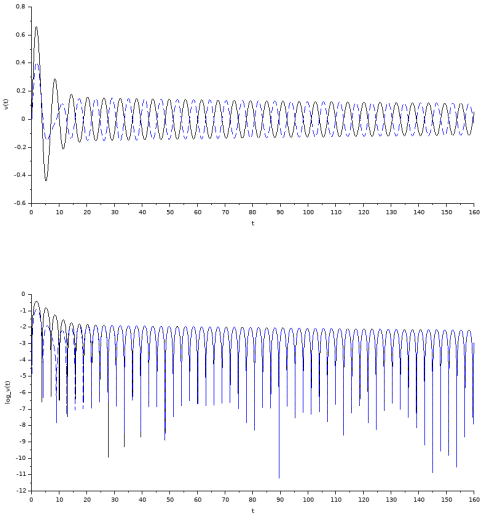

Figure 10: Two particles in a confining potential, evolution of the velocities II (Table 5-Test 2)

When there is no external potential, we observe a large variety of scenario. Again, this can already be understood by considering only 2 particles. In Fig. 12, we show the situation where two particles meet at some point, but the potential

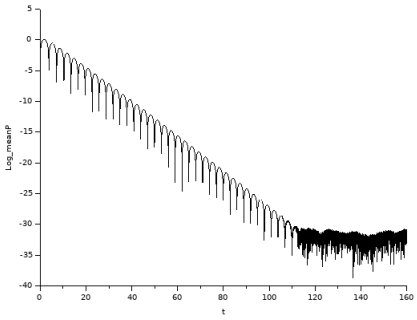

Figure 11: Two particles in a confining potential, evolution of the mean velocity (Table 5-Test 2)

created by their interaction is not strong enough compared to their kinetic energy so that they just cross, and they continue their motion as if they were alone, being stopped by the damping far away from the meeting point. In this situation, their large time behavior looks like as if each particle were alone, with velocities tending exponentially fast to 0, see Fig. 13. We repeat the same simulation, just changing the kinetic energy of the two particles into a far smaller value, see Fig. 14: now, the two particles stay confined in the same neighborhood. They are going back and forth in the common well they are creating themselves; they cross each other, going in opposite directions, with one particle in each side of the potential well. Note that according to the phase portrait in Fig. 15 and the evolution of the velocities in Fig. 16, it is not clear at all, on the time scale of observation, whether the damping effect leads to the full stop at the same point of the two particles or the dynamic tends to a periodic solution. The data for this simulation are collected in Table 6.

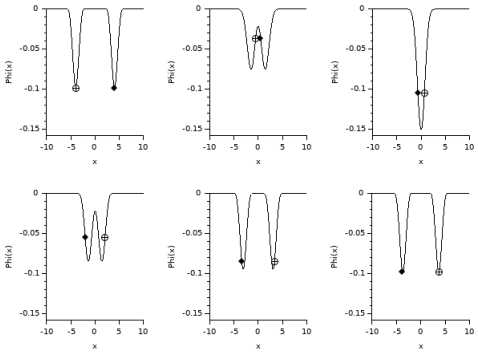

Figure 12: Two particles: weak interaction (Table 6-Test 1)

The complexity of the possible large time scenario increases for larger N's. The space-repartition of the N particles can be complicated and highly depend on the initial state; nonetheless, it is still reasonable to expect that the velocities vanish for large times. However, the rate of conver-

Table 5
Data for the 2-particles simulations with a confining potential

	$W(x)$	c	T	L	Δt	Δx	Δr	q_0^1	p_0^1	q_0^2	p_0^2
Test 1	$.3x^2$	.5	160	3	2.10^{-2}	3/128	2/128	-1	0	1	0
Test 2	$.3x^2$	.5	160	3	2.10^{-2}	3/128	2/128	-1	0	-.75	0

Table 6
Data for the 2-particles simulations with no external force

	$W(x)$	c	T	L	Δt	Δx	Δr	q_0^1	p_0^1	q_0^2	p_0^2
Test 1	0	.5	40	20	2.10^{-2}	20/512	2/128	-4	1	4	-1
Test 2	0	.5	80	20	2.10^{-2}	20/512	2/128	-4	.8	4	-.8

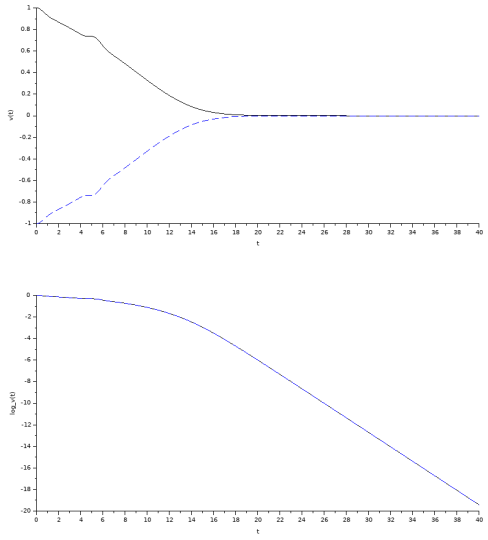

Figure 13: Two particles: weak interaction (Table 6-Test 1), evolution of the velocities

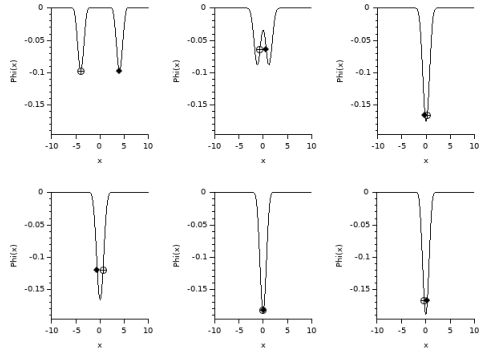

Figure 14: Two particles: strong interaction (Table 6-Test 2)

gence to zero is not exponential. Again, we refer the reader to [35] for an attempt identifying conditions (for the free-space problem) that lead to a final stop of all particles, with a rate which gets slower as N becomes larger. In particular, exploring the large time behavior for the N-particles

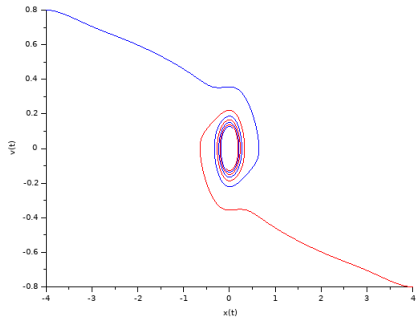

Figure 15: Two particles: strong interaction, phase portrait (Table 6-Test 2)

system becomes numerically demanding, since it requires a long time to establish. Fig. 17 illustrates a case with the creation of a common well: the particles keep moving back and forth along the walls of the well, and the well itself move. Like with one particle, we observe that the medium acts as a friction on the particles cloud, but, considering the particles individually, it is not clear at all whether they will be stopped or kept moving in the common well. In Fig. 18 we see the exponential decay of the mean velocity of the particles until the cloud is stopped. Again, it is not clear whether or not particles will be individually stopped. In contrast to the 2 particles case, we do not observe self-organization of the particles in phase opposition patterns; and after the rapid transient stage, the decay is not anymore exponential. For the presented simulation, we have set the parameters as in Table 7.

We have performed a few simulations adopting the mean-field rescaling, but we do not observe significantly different results.

6.3. Simulations for the Vlasov equation

We turn to (7a)–(7b) and we wish to illustrate numerically Theorem 5. We make use of the parameters in Table 8.

In Fig. 19-left this is the case where c is large enough (Test 1), and Landau damping holds: we see the exponential decay of the macroscopic density and of the self-consistent force. We also observe that the behavior of the particle dis-

Table 7
Data for the N-particles simulations

$W(x)$	c	T	L	Δt	Δx	Δr	N
0	2	40	20	2.10^{-2}	20/512	2/128	100

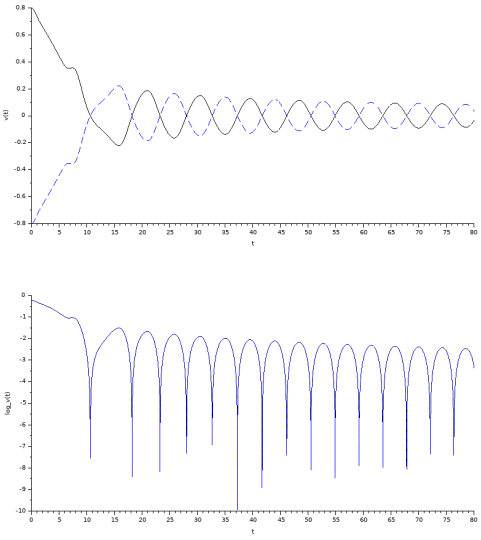

Figure 16: Two particles: strong interaction (Table 6-Test 2), evolution of the velocities

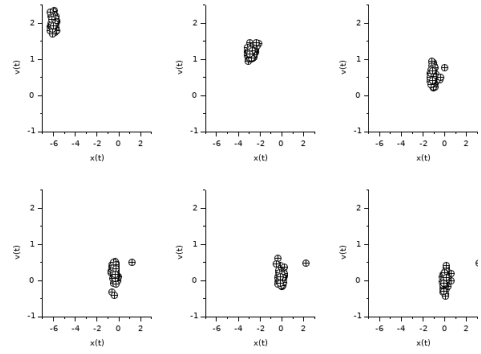

Figure 17: N-particles, evolution of a cloud (Table 7)

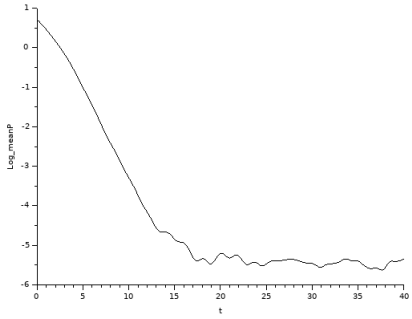

Figure 18: N-particles, evolution of the mean velocity (Table 7)

tribution function is driven for large times by free transport.

In Fig. 19-right and Fig. 20, c is smaller and the Landau damping does not hold (Test 2). We refer the reader to [21] for a link between the wave speed threshold and Jean's length in the attractive Vlasov-Poisson case.

We also illustrate the role of the dimension n for the wave equation. The results depicted in Fig. 21 and Fig. 22 have been obtained with the one-dimensional wave equation (Test 3). There is no damping at all, even increasing the value of c: the particles aggregate, with increased velocities, in a well which is going deeper and deeper. The amplitudes of both the potential and its gradient become larger as time grows. We refer the reader to Appendix A for an explanation of the difference between the cases $n = 1$ and $n = 3$.

The linear stability criterion mentioned in Theorem 5 is not very explicit; one may wonder what is meant in practical terms by this condition and how we can decide easily whether or not a given equilibrium is stable. We have already seen that the answer depends of the value of the parameter c: for a given profile, if c is large enough there is damping (Test 1) whereas for c small enough there is not (Test 2). The question can be addressed the other way around, keeping the value of c fixed. In [21] we have shown that for any given velocity profile $v \mapsto \mathscr{M}(v)$, if the mass of this profile is spread enough, then the linear stability criterion is satisfied. This can be understood by introducing the following rescaling: $\mathscr{M}_\lambda(v) = \lambda^d \mathscr{M}(\lambda v)$. For λ small enough this equilibrium is stable and if λ is large enough the equilibrium is no more stable. Since this rescaling is mass invariant, this result shows that any profile $\mathscr{M}$ of arbitrary large L^1-norm is stable as soon as its mass is spread enough. We can investigate this result at the numerical level as well. We perform several simulations, by making the rescaling parameter λ vary, with the following rescaled initial data

$$F_0^\lambda(x,v) = \lambda Z\left(1 + a\cos\left(\frac{2\pi}{L}x\right)\right)\exp(-\lambda^2 v^2/2).$$

and using the data in Table 9.

Since the parameter λ dilates in velocity the initial data, we can use for the fourth test a smaller computational domain ($V_{\max} = 0.7$) whereas in the sixth test we have to use a larger domain ($V_{\max} = 14$).

In Fig. 23 this is the case where from a stable state (Test 1) we pass to an unstable state by contracting the mass of the velocity profile (Test 4). We see that, since almost all the mass is now concentrated near 0, any spatial perturbation

Table 8
Data for the kinetic simulations, I

	$W(x)$	c	n	T	L	Δt	Δx	Δr	Δv
Test 1	0	0.5	3	60	4	2.10^{-2}	4/256	2/128	7/256
Test 2	0	0.05	3	60	4	2.10^{-2}	4/256	2/128	7/256
Test 3	0	0.5	1	60	4	2.10^{-2}	4/256	2/128	7/256

Table 9
Data for the kinetic simulations, II

	$W(x)$	c	λ	n	T	L	Δt	Δx	Δr	Δv
Test 4	0	1	10	3	60	4	2.10^{-2}	4/256	2/128	0.7/256
Test 5	0	0.1	1	3	60	4	2.10^{-2}	4/256	2/128	7/256
Test 6	0	0.1	0.25	3	60	4	2.10^{-2}	4/256	2/128	14/512

(even small) of this profile creates spatial region where particles are trapped. Conversely, starting from an unstable state (Test 5 and Fig. 24-left) it is possible to obtain a stable state by dilating the velocity profile (Test 6 and Fig. 24-right). In particular this procedure allows us to obtain numerically the Landau damping effect for an arbitrarily small value of c. Nevertheless, this procedure leads to numerical difficulties. On the one hand, for c small the dispersion in the membranes is really slow and the damping rate is small (compare Fig. 19 and Fig. 24-right). Therefore, in order to observe the damping numerically we have to perform computations on a large time interval, which becomes demanding. On the other hand, this procedure dilates in velocity the initial data which thus requires to compute on a larger domain in velocity and increases the computational cost. These two difficulties combine and lead to really heavy simulation. (This is the reason why we perform simulations with $c = 0.1$ and not $c = 0.05$.)

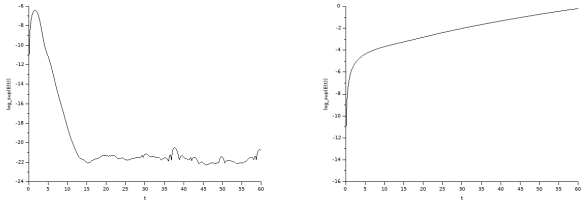

Figure 19: Kinetic model, evolution of the force field (Table 8): the case with c large enough (Test 1: left), and the case $c \ll 1$ (Test 2: right)

7. Conclusion

In this paper, we set up a numerical strategy that preserves accurately the dynamics of energy exchanges for open systems where particles transfer energy to their environment, represented as a transverse vibrational field. The method applies for N-particles model as well as for statistical description based on kinetic equations. In a forthcoming work, it will be applied to quantum particles as well.

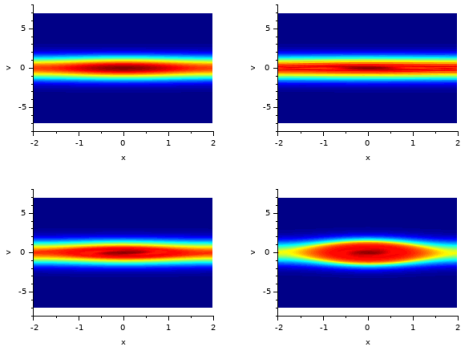

Figure 20: Kinetic model: the case $c \ll 1$ (Table 8, Test 2), the particles distribution function F at several times (top left: initial condition)

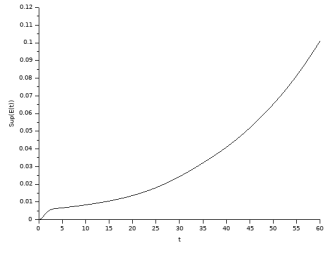

Figure 21: The case $n = 1$ (Table 8, Test 3): the force field

The simulations illustrate the theoretical results obtained when considering a single particle [5], interpreted as a friction effect of the environment on the particle, or many particles [22], where the interaction leads to Landau damping effects. The numerical investigation also sheds light on the role of the parameters of the model; in particular the wave speed c and the dimension n of the vibrational space should satisfy conditions for the damping to occur.

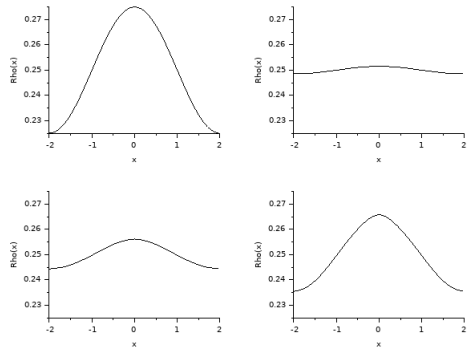

Figure 22: The case $n = 1$ (Table 8, Test 3): the macroscopic density ρ at several time (top left: initial condition)

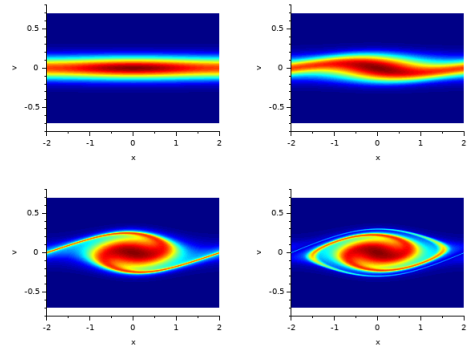

Figure 23: Kinetic model: the case $c = 1$ and $\lambda = 10$ (Table 9, Test 4)

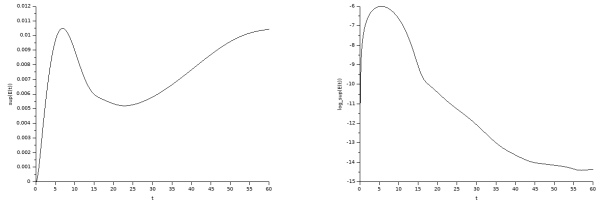

Figure 24: Kinetic model, evolution of the force field: with $c = 0.1$ and $\lambda = 1$ (Table 9, Test 5: left) and $c = 0.1$ and $\lambda = 0.25$ (Table 9, Test 6: right)

A. The case $n = 1$

According to [9], the system (7a)–(7b) can be rewritten as a Vlasov equation with a memory term in the force field

$$\partial_t F + v \cdot \nabla_x F - \nabla_x \left(\Phi_0 - \int_0^t p_c(t-\tau) \Sigma \star \rho(\tau) \, \mathrm{d}\tau \right) \cdot \nabla_v F = 0. \tag{30}$$

In (30), we have $p_c(t) = \int \sigma_2(z) \Upsilon(t,z) \, \mathrm{d}z$ where Υ is the unique solution of the wave equation with initial impulsion σ_2:

$$(\partial_{tt}^2 - c^2 \Delta_z) \Upsilon(t,z) = 0,$$
$$(\Upsilon, \partial_t \Upsilon)\Big|_{t=0} = (0, \sigma_2).$$

In [9, Lemma 14] and [21, Lemma 2.1] it is shown that the kernel p_c satisfies the following properties.

Proposition 10. *For $n \geq 3$, $p_c \in L^1(0, +\infty)$ and*

$$\int_0^{+\infty} p_c(t) \, \mathrm{d}t = \frac{\kappa}{c^2} \quad ; \quad \kappa = \int \frac{|\widehat{\sigma}_2(\zeta)|^2}{|\zeta|^2} \, \mathrm{d}\zeta.$$

If, moreover, n is odd, then p_c has a compact support included in $[0, 2R_2/c]$ (with $\mathrm{supp}(\sigma_2) = B(0, R_2)$) and

$$|p_c(t)| \lesssim \frac{\|\sigma_2\|_{L_z^{2n/(n+2)}} \|\sigma_2\|_{L_z^2}}{c}.$$

That κ is finite clearly relies on the assumption $n \geq 3$. This statement means that there is a loss of memory effect in the force field of (30). This loss of memory effect is an important mechanism in the analysis [21] of the Landau damping for (7a)–(7b). In dimension $n = 1$ there is no such a loss of memory effect in the kernel p_c. In turn, if the initial data has a spatial inhomogeneity, then the force field created by the medium cannot be damped and the force field eventually grows in the spatial region where the force field acted initially as an attractive force.

Proposition 11. *If $n = 1$, then $p_c(t) \geq 0$ and $\lim_{t\to\infty} p_c(t) = \frac{1}{2c} \|\sigma_2\|_{L_z^1}^2$.*

This proposition is a direct application of the d'Alembert formula:

$$\Upsilon(t,z) = \frac{1}{2c} \int_{z-ct}^{z+ct} \sigma_2(s) \, \mathrm{d}s$$

which allows us to obtain

$$p_c(t) = \frac{1}{2c} \int_{-\infty}^{+\infty} \sigma_2(z) \left(\int_{z-ct}^{z+ct} \sigma_2(s) \, \mathrm{d}s \right) \mathrm{d}z.$$

This is precisely the effect illustrated in Fig. 21 and 22: assuming $n \geq 3$ is not a matter of technical difficulty, but is deeply related to the physical mechanisms described by the model.

Acknowledgements

We are gratefully indebted to S. de Bièvre for many stimulating discussions and warm encouragements. We also thank A. Vavasseur for having let us be aware of the recent developments in [35].

References

[1] B. Aguer, S. De Bièvre, P. Lafitte, and P. E. Parris. Classical motion in force fields with short range correlations. *J. Stat. Phys.*, 138(4-5):780–814, 2010.

[2] G. Allaire. *Analyse numérique et optimisation*. Editions de l'École Polytechnique, 2012.

[3] J. Bedrossian, N. Masmoudi, and C. Mouhot. Landau damping: paraproducts and Gevrey regularity. *Ann. PDE*, 2(1):Art. 4, 71, 2016.

[4] J. Bedrossian, N. Masmoudi, and C. Mouhot. Landau damping in finite regularity for unconfined systems with screened interactions. *Comm. Pure Applied Math.*, 71(3):537–576, 2018.

[5] L. Bruneau and S. De Bièvre. A Hamiltonian model for linear friction in a homogeneous medium. *Comm. Math. Phys.*, 229(3):511–542, 2002.

[6] A. O. Caldeira and A. J. Leggett. Path integral approach to quantum Brownian motion. *Physica A*, 121:587–616, 1983.

[7] A. O. Caldeira and A. J. Leggett. Quantum tunnelling in a dissipative system. *Ann. Phys.*, 149:374–456, 1983.

[8] S. De Bièvre, J. Faupin, and B. Schubnel. Spectral analysis of a model for quantum friction. *Rev. Math. Phys.*, 29(6):1750019, 49, 2017.

[9] S. De Bièvre, T. Goudon, and A. Vavasseur. Particles interacting with a vibrating medium: existence of solutions and convergence to the Vlasov–Poisson system. *SIAM J. Math. Anal.*, 48(6):3984–4020, 2016.

[10] S. De Bièvre, T. Goudon, and A. Vavasseur. Stability analysis of a Vlasov–Wave system describing particles interacting with their environmemt. *J. Diff. Eq.*, 264(12):7069–7093, 2018.

[11] S. De Bièvre, P. Lafitte, and P. E. Parris. Normal transport at positive temperatures in classical Hamiltonian open systems. In *Adventures in mathematical physics*, volume 447 of *Contemp. Math.*, pages 57–71. Amer. Math. Soc., Providence, RI, 2007.

[12] S. De Bièvre and P. E. Parris. Equilibration, generalized equipartition, and diffusion in dynamical Lorentz gases. *J. Stat. Phys.*, 142(2):356–385, 2011.

[13] S. De Bièvre, P. E. Parris, and A. Silvius. Chaotic dynamics of a free particle interacting linearly with a harmonic oscillator. *Phys. D*, 208(1-2):96–114, 2005.

[14] B. Engquist and A. Majda. Absorbing boundary conditions for the numerical simulation of waves. *Math. Comput.*, 31(139):629–651, 1977.

[15] E. Faou, R. Horsin, and F. Rousset. On numerical Landau damping for splitting methods applied to the Vlasov-HMF model. *Foundations Comput. Math.*, 18(1):97–134, 2018.

[16] F. Filbet and E. Sonnendrücker. Comparison of Eulerian Vlasov solvers. *Computer Physics Communications*, 150(3):247–266, 2003.

[17] F. Filbet and E. Sonnendrücker. Numerical methods for the Vlasov equation. In F. Brezzi, A. Buffa, S. Corsaro, and A. Murli, editors, *Numerical Mathematics and Advanced Applications*, pages 459–468. Springer Milan, 2003.

[18] F. Filbet, E. Sonnendrücker, and P. Bertrand. Conservative numerical schemes for the Vlasov equation. *J. Comput. Phys.*, 172:166–187, 2001.

[19] J. Fröhlich, Z. Gang, and A. Soffer. Friction in a model of Hamiltonian dynamics. *Comm. Math. Phys.*, 315(2):401–444, 2012.

[20] T. Goudon. *Mathematics for modeling and scientific computing*. Mathematics and Statistics Series. ISTE, London; John Wiley & Sons, Inc., Hoboken, NJ, 2016.

[21] T. Goudon and A. Vavasseur. Mean field limit for particles interacting with a vibrating medium. *Annali Univ. Ferrara*, 62(2):231–273, 2016.

[22] T. Goudon and L. Vivion. Landau damping in dynamical Lorentz gases. Technical report, Univ. Côte d'Azur, Inria, CNRS, LJAD, 2019. Available at https://hal.archives-ouvertes.fr/hal-02155761.

[23] W. Guo and J.-M. Qiu. Hybrid semi-Lagrangian finite element-finite difference methods for the Vlasov equation. *J. Comput. Phys.*, 234(0):108–132, 2013.

[24] E. Hairer, C. Lubich, and G. Wanner. *Geometric numerical integration*, volume 31 of *Springer Series in Computational Mathematics*. Springer, Heidelberg, 2010. Structure-preserving algorithms for ordinary differential equations, Reprint of the second (2006) edition.

[25] A. Komech, M. Kunze, and H. Spohn. Effective dynamics for a mechanical particle coupled to a wave field. *Comm. Math. Phys.*, 203(1):1–19, 1999.

[26] A. Komech, H. Spohn, and M. Kunze. Long-time asymptotics for a classical particle interacting with a scalar wave field. *Comm. Partial Differential Equations*, 22(1-2):307–335, 1997.

[27] P. Lafitte, P. E. Parris, and S. De Bièvre. Normal transport properties in a metastable stationary state for a classical particle coupled to a non-Ohmic bath. *J. Stat. Phys.*, 132(5):863–879, 2008.

[28] C. Mouhot and C. Villani. On Landau damping. *Acta Math.*, 207(1):29–201, 2011.

[29] J.-M. Qiu and C.-W. Shu. Conservative semi-Lagrangian finite difference WENO formulations with applications to the Vlasov equation. *Comm. Comput. Phys.*, 10:979–1000, 2011.

[30] J.-M. Qiu and C.-W. Shu. Positivity preserving semi-lagrangian discontinuous Galerkin formulation: Theoretical analysis and application to the Vlasov–Poisson system. *J. Comput. Phys.*, 230:8386–8409, 2011.

[31] J. M. Sanz-Serna and M. P. Calvo. *Numerical Hamiltonian problems*, volume 7 of *Applied Mathematics and Mathematical Computation*. Chapman & Hall, London, 1994.

[32] E. Soret and S. De Bièvre. Stochastic acceleration in a random time-dependent potential. *Stochastic Process. Appl.*, 125(7):2752–2785, 2015.

[33] T. Umeda. A conservative and non-oscillatory scheme for Vlasov code simulations. *Earth Planets Space*, 60:773–779, 2008.

[34] T. Umeda, M. Ashour-Abdalla, and D. Schriver. Comparison of numerical interpolation schemes for one-dimensional electrostatic Vlasov code. *J. Plasma Physics*, 72:1057–1060, 2006.

[35] A. Vavasseur. Long time behaviour of interacting particles through a vibrating medium: comparison between the N-particle system and the natural kinetic equation dynamics. Technical report, BCAM, Bilbao, Spain, 2019. Available at the URL https://hal.archives-ouvertes.fr/hal-02012981.

[36] M. P. Velasco, D. Usero, S. Jiménez, and L. Vázquez. Transparent boundary condition for the wave equation in one dimension and for a Dirac like equation. *Electronic J. Diff. Equ.*, Conference 22:117–137, 2015. Madrid Conference on Applied Mathematics in honor of Alfonso Casal.

[37] E. Zampieri and L. F. Pavarino. Implicit spectral element methods and Neumann-Neumann preconditioners for acoustic waves. *Comput. Methods Appl. Mech. Engrg.*, 195(19–22):2649–2673, 2006.